ABSTRACT

EVAPORATING CROSS FLOW SPRAY JETS IN GAS-SOLID CIRCULATING FLUIDIZED BED

by
Tong Hoon Lee

Three-phase flow of solid-gas suspension with liquid spray is found in many industrial applications, including fluidized catalytic cracking in petroleum refinery process, and wet scrubbing process. This dissertation study is aimed to understand the gas-solid-liquid three-phase flow structure, phase interactions and transport in a gas-solid circulating fluidized bed where an evaporating cross-flow liquid spray jet from a rectangular nozzle with a fan angle is injected. The investigation is based on both numerical and experimental approaches. The numerical study is for detailed field descriptions of the flow structure, phase interaction and distributions whereas the experimental study is for simulation validations. The numerical simulation further explores the parametric effects such as nozzle aspect ratio and solids loading on the spray structure, evaporation characteristics as well as local phase distributions of solid concentration, gas temperature and velocity. The governing equations of both gas and solids phases are solved by the Eulerian method while the droplet phase is modeled by the Lagrangian approach. For the experimental validation of numerical simulations, a circulating fluidized bed (CFB) has been set up with a thermocouple matrix system for phase temperature measurement. Cases of liquid nitrogen spray jets from rectangular nozzles with aspect ratio up to 4 in cross-flows of air–FCC suspensions with solids volumetric fraction up to 25% in the CFB system at ambient conditions were numerically investigated. Experimental validations for aspect ratio up to 4 and solids volumetric fraction up to 1.5% were performed.

The results show that the spray penetrates basically along its injection fan angle but deflected by the gas-solid cross-flow convection. The penetration length is significantly reduced by the increase in solids loading. Due to the strong cross-flow convection, most vaporized gas is blown away from the spray region, as indicated by the deviation of the gas and solids' velocity and temperature contours. The results also show that the spray evaporation leads to a very low solids concentration within the vapor region while there is a dense layer of solids surrounding the vapor region. Detailed droplet structure along the trajectory and field distributions of velocity, temperature and concentration of gas and solids were also obtained. With low solids concentrations, there exist flow similarities in velocity and temperature distributions in the spray region. As expected, the flow structure is also strongly dependent on the nozzle orientation, with a deeper penetration and less deflection of vertically-oriented rectangular nozzle than that of a horizontally-orientated nozzle. The simulation predictions agree reasonably well with the experimental measurements.

EVAPORATING CROSS FLOW SPRAY JETS IN GAS-SOLID CIRCULATING FLUIDIZED BED

by
Tong Hoon Lee

A Dissertation
Submitted to the Faculty of
New Jersey Institute of Technology
in Partial Fulfillment of the Requirements for the Degree of
Doctor of Philosophy in Mechanical Engineering

Department of Mechanical Engineering

May 2005

APPROVAL PAGE

EVAPORATING CROSS FLOW SPRAY JETS IN GAS-SOLID CIRCULATING FLUIDIZED BED

Tong Hoon Lee

Dr. Chao Zhu, Dissertation Advisor — Date
Professor of Mechanical Engineering, NJIT

Dr. Teh C. Ho, Committee Member — Date
Senior Research Associate, ExxonMobil Research & Engineering Co., Annandale, NJ

Dr. Rong-yaw Chen, Committee Member — Date
Professor of Mechanical Engineering, NJIT

Dr. Ernest S. Geskin, Committee Member — Date
Professor of Mechanical Engineering, NJIT

Dr. Rajesh N. Dave, Committee Member — Date
Professor of Mechanical Engineering, NJIT

BIOGRAPHICAL SKETCH

Author: Tong Hoon Lee

Degree: Doctor of Philosophy

Date: May 2005

Undergraduate and Graduate Education:

- Doctor of Philosophy in Mechanical Engineering,
  New Jersey Institute of Technology, Newark, NJ, 2005

- Master of Science in Mechanical Engineering,
  Korea University, Seoul, Korea, 1993

- Bachelor of Science in Mechanical Engineering,
  Korea University, Seoul, Korea, 1991

Major: Mechanical Engineering

Presentations and Publications:

Lee, Tong H., Wang, Xiaohua and Zhu, Chao,
"3-D simulation of cross-flow evaporating sprays in circulating fluidized beds"
The 8th International Conference on Circulating Fluidized Beds
Hangzhou, China May 2005

Lee, Tong H. and Zhu, Chao,
"Numerical simulation of evaporating cross flow sprays in gas-solid circulating fluidized beds"
Journal of the Chinese Institute of Chemical Engineers, Vol. 36, No. 1, pp. 43-48, January 2005.

Lee, Tong H. and Zhu, Chao,
"3-D simulation of an evaporating cross flow spray in a gas –solid circulating fluidized bed"
The 9th Asian Conference on Fluidized-Bed and 3-phase Reactors, Wanli, Taiwan, November 2004.

Lee, Tong H. and Zhu, Chao,
"3-D simulation of cross flow evaporating sprays in circulating fluidized beds" Frontiers in Applied and Computational Mathematics (FACM'04), Newark, NJ, May 2004.

Qureshi, M. M. R., Lee, Tong H., Yu, Qun and Zhu, Chao,
"Evaporating spray jets in cross-flow gas-solids suspensions:effects of aspect ratios of rectangular nozzles"
2003 AICHE Annual Meeting, San Francisco, CA, November 2003

Rossetti, Jr., G. A., Pinceloup, P., Oledzka, M., Suchanek, W., Mikulka-Bolen, K., Lencka, M. M., Emre, M., Lee, T., Zhu, C., Dave, R. McCandlish, L. E. and Riman, R. E.
"Hydrothermal Growth of Epitaxial PZT"
204th Meeting of The Electrochemical Society, Orlando, FL, October 2003.

To my beloved family

My wife, Jee Eun Oh

My sons, Kenneth and Aidan

ACKNOWLEDGMENT

I wish to acknowledge the stimulus and support of many individuals in the development of this thesis. First, my deepest appreciation is expressed to Dr. Chao Zhu, who not only guided me with remarkable insight and intuition in every instance as my supervisor but also gave me friendship, inspiration and persistent encouragement throughout this research. Secondly, my committee members, Dr. Teh C. Ho, Dr. Rong-yaw Chen, Dr. Ernest Geskin and Dr. Rajesh N. Dave deserve many thanks for reviewing this thesis and the actively participating in my committee.

I am grateful to my laboratory senior Dr. Joshua Wang who basically completed the code that contributed much in my research progress and supported me kindly even in his working hours. Thanks to my fellows Qun Yu and Muhamad in the Particulate Multiphase Fluids Engineering Laboratory for their support. I appreciate the friendship of Dr. Gary Liu, who always kindly gave me advices during my study.

I acknowledge the supports from Department of Mechanical Engineering, New Jersey Institute of Technology for TA scholarship and partial support of Exxon Mobil Research & Engineering Company under the NJIT Research Grant No. 998314.

Last but not the least, I would especially like to thank to Dr. Chao-Shin Lin in Boeing Company who had instructed me numerical code for two years as my co-advisor.

TABLE OF CONTENTS

TABLE OF CONTENTS
(Continued)

Chapter **Page**

Chapter **Page**

LIST OF TABLES

LIST OF FIGURES

LIST OF FIGURES

LIST OF FIGURES

LIST OF SYMBOLS

Symbols	Meaning
A	area
C_d	drag coefficient
C_p	specific heat
D	diffusivity
d	diameter
Gr	Grashof number
g	gravity
H	heat transfer rate
h	heat transfer coefficient
I	momentum transfer
m	mass
$\dot{m}$	Evaporation rate of a droplet or mass flux
Nc	number of contacts of the active particles with neighboring particles
Nu	Nusselt number
Pr	Prantdl number
p	pressure
q	heat flux
Re	Reynolds number
r	radius
S	stress

T	temperature
t	time
v	velocity
W	molecular weight
x	location coordinate
y	mass fraction

Greek letters

β	thermal expansion coefficient
ε	volume fraction
Γ	volumetric evaporation rate
ρ	density

Subscript

0	initial or standard
∞	infinite
a	active
b	bed
c	collision
d	droplet
eff	effective
g	gas

m	mixture excluding vapor
mf	minimum fluidization
p	particle
s	solid
v	vapor

CHAPTER 1

INTRODUCTION

Three phase mixed flow of solid-gas suspension with liquid spray is used in many industrial applications. Typical example is the mixing and vaporization of crude oil in the suspended catalytic particle flow in the Fluidized Catalytic Cracking (FCC) unit. Heavy oil is injected through the feed nozzle; droplet evaporates immediately upon collision with hot catalytic particles; oil vapor is quickly absorbed into the porous channels of the catalytic particle where cracking occurs; significant heat transfer accompanies the process of vaporization and cracking; within the unit (Figure 1.1). The most complicated feature is the three-phase coupling among these phase transport processes.

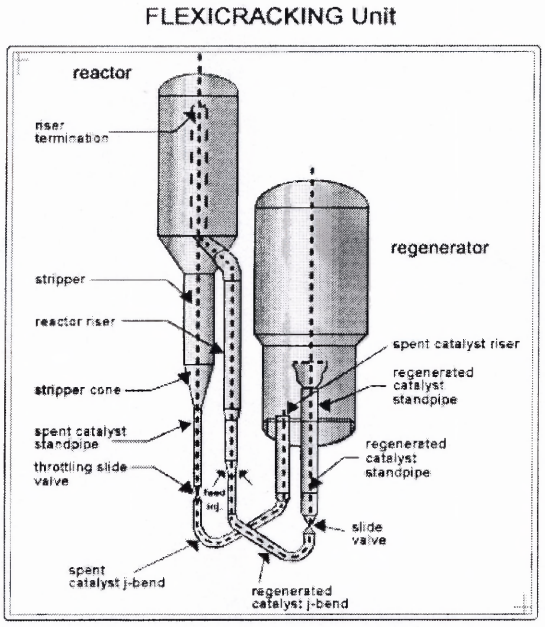

Figure 1.1 Riser cracking FCC unit (Kunii and Levenspiel, 1991).

Another example is a polymerization reaction process. Large amount of heat is generated over a short period of time during the reaction process (Figure 1.2). In order to relieve the reactor from the excessive heat, an evaporative liquid of monomers is injected into the reactor. Consequently the evaporated vapor from liquid spray jets depletes local phase temperature; dilutes solid concentration and changes phase velocities, which leads to the modulation of fluidized bed behavior in the reactor. Hence, the evaporating fluid absorbs the excessive heat; provides additional reactants (monomers); and adjusts the reaction rate.

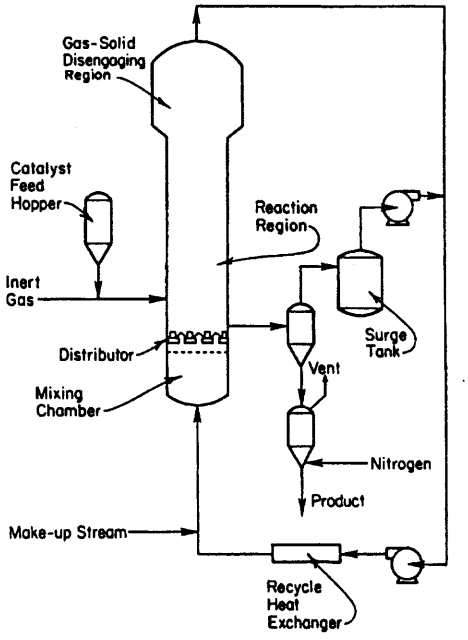

Figure 1.2 Condensed mode operation for polymerization process (Jenkins et al., 1986).

Other applications include wet scrubbing (Figure 1.3), particle nucleation, agglomeration, and coating.

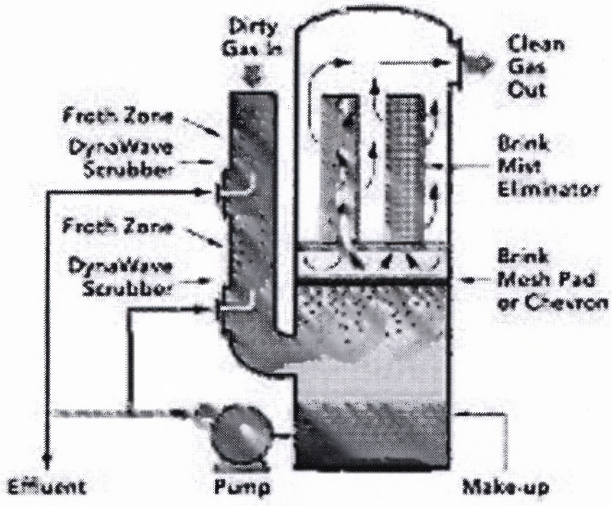

Figure 1.3 Environmental cleaning of suspended particulate by wet scrubbing (DynaWave/Brink®).

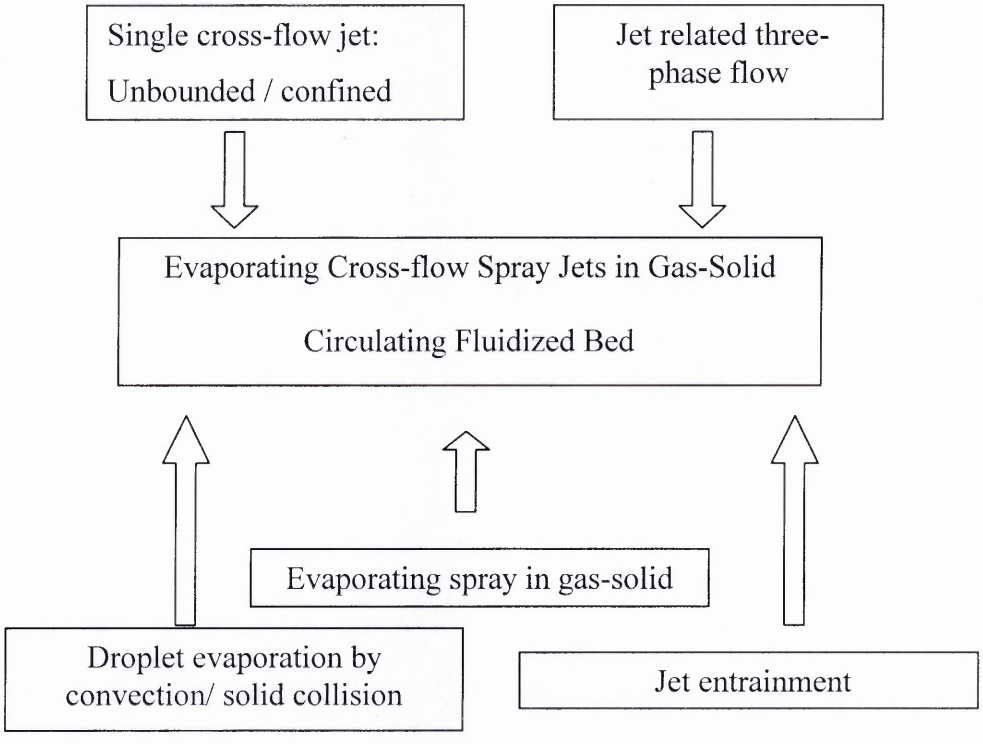

Figure 1.4 Sub-categories related to the thesis topic.

Although there are many usages in industries, very limited research in the field of solid-gas suspension flows with liquid sprays (especially with evaporation), either numerically or experimentally, has been reported so far. Mostly needed but not well-known phenomena are spray structures and spray vaporization characteristics in gas-solid suspensions under diverse process conditions. So the main objectives of this study are targeted at these problems. Figure 4 outlines the approach used in this study.

Evaporating liquid spray jets in gas-solid suspensions are characterized by the strong three-phase interactions with momentum, heat and mass transfer across the phase boundaries. Designing an optimal nozzle for these applications is non trivial due to the fact that it is not easy to optimize all of the spray jets' characteristics for a given nozzle configuration. In the FCC applications, the rectangular nozzles are typically used due to their wide spread range and as well as their mass and momentum conservations are quite different than circular counterparts. In this regard, both numerical and experimental studies are carried out to investigate the most unique characteristics of the evaporating spray jets with rectangular nozzles in the gas-solid cross-flows in circulating fluidization systems. Because the numerical study aims to better understand the phase interaction aspects that are difficult to characterize experimentally. The simulation portion of this study attempts to explore the parametric effects of parameters (such as nozzle aspect ratio and spray jet characteristic) on local phase distributions (such as solid concentration, temperature and velocity), the in-bed spray structure as well as spray evaporation characteristics.

The governing equations of gas-solid-liquid three phase flows are implemented with strong phase-phase interactions and interfacial transfers. The governing equations of

both gas and solids phases are solved by the Eulerian method while the droplet phase is modeled by the Lagrangian approach. Specifically, study focuses on the effects of ambient solid loading on spray evaporation and mixing as well as the effects of droplet evaporation on temperature depletion and dilution of solid concentration. Nozzle aspect ratios up to 4 and vertical orientation on the jet penetration as well as jet deflections were also investigated.

For the convenience of experimental study, a test loop with an operational mode in circulating fluidized bed (CFB) has been set up. Thermocouple measurement module is implemented to determine the spray structure in a gas-solid flow. In this study rectangular liquid nitrogen (LN2) spray jets were used in cross-flows of air–FCC suspensions at ambient conditions.

CHAPTER 2

LITERATURE SURVEY

2.1 Single Phase Cross-flow Jet

Theoretical understanding on co-flow one-phase jets is well known, where jet regimes and flow similarities are extensively studied. In the one-phase cross-flow jets, the development of kidney-shaped contour with paired counter-rotating vortices of the bending jets makes the jet structure very complicated, as shown in Figure 2.1. The existence of the pair vortices may reach to a very far field, up to a distance of 1000 nozzle diameters, with a growing size but a decreasing intensity [Pratte and Baines, 1967]. Some similarities in velocity and pressure distributions in a region near the nozzle may still exist whereas the entrainment can be enhanced due to the cross-flow convection [Abramovich, 1963].

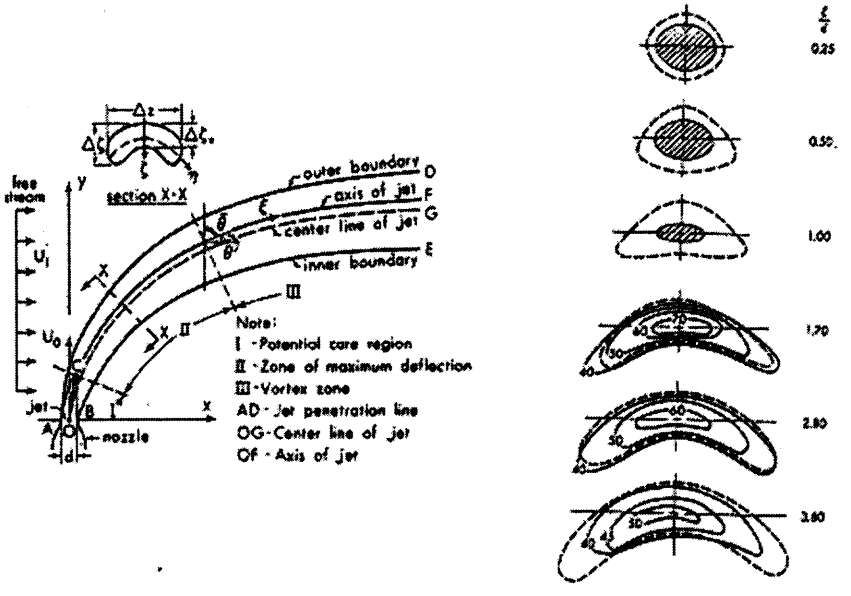

Figure 2.1 Characteric contours of cross-flow jet [Abramovich, 1963].

2.2 Jet Related Two-phase Flow

Jet related two-phase flows have been studied extensively over the past few decades. Many researchers simulated the droplet evaporation and spray dynamics with partial verifications from experimental measurements. For example, for a gas-liquid jet into an unbounded concurrent gas flow, the jet boundary expansion was formulated [Abramovich, 1963]. In addition, the entrainment rate can be significantly reduced, whereas the jet boundary is further expanded due to gas phase expansion by combustion or evaporation [Ricou and Spalding, 1961].

A mathematical model of a gas-droplet non-isothermal multi-component poly-disperse turbulent jet was proposed based on a multi-fluid concept by solving Eulerian governing equations [Zuev, Lepeshinskii, 1995]. Eulerian-Lagrangian stochastic method was applied to the dilute evaporating spray in a co-flowing, turbulent heated air stream [Chen and Pereira, 1995; 1996]. The model shows that the droplet mass fluxes persistently accumulate near the centerline region. The spray and droplet behavior in terms of fluid dynamics and transport phenomena with both theoretical and computational aspects was addressed [Sirignano, 1999].

2.3 Droplet Evaporation by Convection and Solid Collision

Many studies on evaporative spray jet in particle free environment have been reported. These studies are typically focused on the droplet generation, evaporation and droplet-droplet interactions. Exponential temperature distributions of the liquid jet along the axial direction were correlated. Dying visualization and image technique was used to study the atomization and vaporization dynamics of liquid methanol in a burning spray jet [Bazile

and Stepowski, 1994]. Local vaporization dynamics was observed and reduction in droplet diameter was correlated. The effect of multi-droplet interactions on evaporation and droplet motion of a dense spray in a hot gas environment was studied [Silverman and Sirignano ,1994] . The phase Doppler method was used to evaluate the effect of droplet collisions on spray mixing [Gavalses *et al.*, 1995]. A model was developed to illustrate of the phase change process of evaporation, in which the fuel spray is divided into three regimes, namely the sheet portion, the break up portion, and the droplet portion [Kouremenous *et al.*, 1995]. The break-up and atomization of a round water jet by a high-speed annular air jet was developed [Lasheras *et al.*, 1998]. The specific flux of kinetic energy supplied by the gas to the spray jet was found to be the primary parameter determining the secondary break-up and coalescence of droplet in the far field.

Several evaporation models of a single droplet have been widely used, such as the d^2 law, the infinite conductivity model, the limited conduction model, and the vortex model. The effect of different models on the evaporation of a single-component droplet in a transient one-dimensional flow of air-fuel droplet mixture was examined [Aggarwal, 1984]. It was shown that both the d^2 law and the infinite conductivity model are not adequate to predict the evaporation behavior in the convective environment. He recommended the spherically symmetric conduction model for low Reynolds numbers and the simplified vortex model for high Reynolds numbers. With multi-component droplet, additional analysis of the liquid-phase mass diffusion is necessary for the prediction rates of each component [Aggarwal *et al.,* 1991; Hallett, 2000]. The effect of turbulence flows on droplet evaporation rate has also been extensively investigated [e.g., Gakkhar & Ppakash, 1990; Michaeledes *et al.* 1992; Haywood, 1994]. The results

showed that the turbulence enhancement elements could be advantageously used for the improvement of phase change process.

Vaporization of a droplet in a spray is often affected by the interaction with its neighboring droplet [Chiang *et al.,* 1992; Silverman & Sirignano, 1994]. The droplet interactions may strongly affect various transport coefficients of the droplet, such as drag coefficient, Nusselt number and Sherwood number. A dense spray model to study the multi-droplet interactions on evaporation and motion of a dense spray in hot gaseous environment was developed. [Silverman, Sirignano, 1994]

2.4 Numerical Approach on Multi Phase Flow

Numerical simulations of oil spray in FCC risers were attempted to reveal detailed field information of three phase flows (Chang *et al.*, 1998; Gao *et al.*, 2001). In these simulations, particle-droplet collisions and some important phase interactions were ignored. For the study of evaporating spray jets in gas-solids flows, different modeling approaches could be selected from the reported literature. One is the continuum multi-fluid method in which each phase of gas, solids or droplet is a pseudo-continuum and the governing equations are solved simultaneously [Crowe, 1984; Chang *et al.*, 1996, 1998; Straatsma *et al.*, 1999]. However, in cases where particles are poly-dispersed and undergoing a phase change along their paths, it is difficult to define the phase and phase interactions that are size sensitive in the continuum approach. In such circumstances, the particles may be treated by the multi-lump method [Lottes *et al.*, 1993], in which particles are separated into a limited number of lumped groups where the particles in each group are of the same size. Since the droplet evaporation rate is a strong function of

droplet size, the multi-lump method may lead to a large biased error in the estimation of droplet evaporation rate. The other approach is the probability density function (PDF) method for the droplet phase [Williams, 1958]. However, no studies have been reported on applying the PDF method to account for the droplet-solids interactions, such as collision that is one of the key effects in the study of liquid spray in a gas-solids flow.

The hybrid Eulerian-Lagrangian method [Ahluwalia, 1999] is another approach in which gas and solids phases are treated by the Eulerian two-phase continuum method, while the droplet phase is treated by the Lagrangian trajectory method. This approach nevertheless requires a number of iterations on phase coupling between the gas-solids two-phase flow and the droplet phase until all phase interactions are converged. It is noted that, in the numerical studies of gas-solids flows, the Lagrangian method is typically used when the flow is dilute [Kawaguchi *et al*, 1998; Senior & Grace, 1998; Lun, 2000], while the Eulerian method is more often used if the flow is a dense suspension. [Sinclair & Jackson, 1989; Joseph *et al.*, 1990] With a simple heat transfer model of droplet-solid collision and phase interaction correlations, Wang *et al.* (2004) performed a combined Eulerian-Lagrangian simulation of a concentric spray in dilute pipe flow. Modeling of other gas-solids-droplet flows with evaporation (such as food drying) may be simplified into two-phase (wet solid and gas) models to avoid three-phase interactions.

2.5 Evaporating Spray Jet in Gas-solid Flows

Few studies of droplet evaporation in a gas-solid flow have been reported, in which many additional important factors control the droplet evaporation phenomena. Research in this

field requires an interactive study of many advanced topics such as dispersion and mixing of two-phase flows, particle-droplet collision, particle-turbulence modulation, and evaporation of liquid droplet. The effect of thermal radiation on single droplet vaporization was addressed [Harpole, 1980; Lage, 1993]. Thermal diffusion was found to be essential to evaporation or combustion of fuel droplet with internal heat sources. Droplet evaporation also affects the droplet-solid collision [Leong *et al.*, 1995], which depends on the heat transfer type, collision time and contacting area. The heating and vaporization of feed droplet in fast catalytic cracking (FCC) risers was analyzed [Buchanan, 1994]. Considering the vapor diffusion of droplet and the effect of particles, he proposed an empirical correlation of heat transfer coefficient for a droplet in the FCC riser.

In an attempt to simulate the hydrodynamic and superheated characteristics of riser reactor, Gu (1995) investigated the evaporation rate of liquid nitrogen spray in the riser. However, his model underestimated the phase-interactions and hence the evaporation rate. The similarity model was developed to estimate the droplet evaporation region based on the jet boundary theory [Zhu *et al.*, 2001]. It was shown that spray structures severely changed by the particle loading on the gas-solid flow. Chang *et al.* (1996; 1998) performed the full field numerical simulation of oil spray in FCC reactors. The hydrodynamic processes of heat transfer, droplet evaporation, and mixing were investigated. However, in his study, the effects of particle-droplet collisions on droplet evaporation were ignored. The similar approach of solving full-coupling Eulerian equations has also been applied for other gas-solid-droplet flows such as food drying process and bio-reactor applications [Crowe, 1983; Straatsma, 1999]. Wang *et al.* (2004)

performed a numerical simulation of a concentric liquid nitrogen spray in a dilute FCC pipe flow, in which the flow similarity is found in the dilute three-phase flows with spray evaporation.

2.6 Nozzle Aspect Ratio and Orientation Angle Effect

The flow field arising from a sharp-edged rectangular jet has been extensively studied [Chang *et al.*, 1996]. Features of the flow arising from a rectangular jet with an aspect ratio of 4 injected into a cross-flow was studied [Weston and Thames, 1979]. Both orientations of the jet relative to the free stream velocity (major axis either normal or parallel to the flow) were investigated in this work. The penetration and deflection is deeply depending on not only the openness but also the aspect ratio and the orientation of the nozzle.

2.7 Summary

While co-flow jets are relatively known, especially for the single-phase flows, the quite different flow characteristics of multiphase cross-flow jets have not been extensively studied. Extensions of flow characteristic relationships of single-phase jets into applications with spray jets in multiphase flows are yet to be verified or modified. Atop of these, the effect of droplet evaporation on jet structure, especially in gas-solids suspensions is barely explored. Effects of aspect ratio of rectangular nozzles on cross-flow spray penetrations, deflection and expansions in gas-solids suspensions has not been explored.

For evaporating cross-flow sprays in solid-gas suspensions, partially due to the lack of reliable experimental results, simple and reliable mechanistic models of droplet-particle collisions and associated phase transport at elevated temperatures have not been developed. Other basic models of topics such as isolated droplet vaporization, heating and acceleration, multi-component liquid droplet, droplet-droplet and droplet-wall collisions, droplet interactions with turbulence and vortical structures need to be implemented into the advanced numerical modeling of such three-phase flows. On the other hand, the overall system-based parametric model requires the detailed phase distributions of gas and solids in the presence of evaporating sprays, which are only obtainable from the sophisticated numerical modeling and simulations.

This study is aimed to numerically explore the flow characteristics of cross-flow spray jets with strong evaporations in gas-solid suspensions at various solids loadings. Particular research interests are on the spray structure (evaporation rate, penetration, deflection and expansion) and phase distributions (e.g., solids concentration, gas temperature, and gas velocity) in the spray region as well as the effect of aspect ratio of rectangular spray nozzles.

CHAPTER 3

NUMERICAL SIMULATION

3.1 Introduction

The main objectives in numerical studies are given as follows. First, trajectories of droplet, solids concentration and temperature distributions as well as gas and solid velocity profiles in gas-solid suspensions with evaporating sprays will be evaluated. Effects of solids loading and nozzle aspect ratios on these phase distributions will be studied. Also interpretation and comparison of these numerical results with experimental results and observations will be carried out. Particularly, some parametric effects on phase field distributions that are difficult to be experimentally investigated will also be investigated via numerical simulations in this study.

3.2 Numerical Simulation Methodology

In this study, the hybrid Eulerian-Lagrangian approach was adopted, namely, the gas-solids suspension flow was calculated using the Eulerian two-fluid model approach, in which the effects of the droplet were coupled through the source terms in the mass, momentum and energy governing equations of each phase. The evaporating spray on the other hand is treated using the deterministic Lagrangian trajectory approach, in which the droplet consist of a finite number of trajectory groups. Droplet evaporate along their trajectories and interact with the surrounding gas-solids suspension along their paths. While the droplet evaporation and trajectory affect the gas-solids flow by the phase interactions, such as the drag forces and droplet-solids collisions, the gas-solids flow field

in turn affects the droplet evaporation and its trajectory. By iterations between these two interacting approaches, a final solution of the three-phase flow is obtained once a convergence is achieved.

3.3 Eulerian Approach for the Gas/Solids Phase

In this study, the modeling of the gas-solids flow is based on the MFIX code that was originally developed by Morgantown Energy Technology Center [Syamlal *et al.*, 1994; Syamlal, 1995]. In the calculation of gas-solids flows, it is assumed that the solids are mono-dispersed without attrition. The gas phase is a mixture of air and nitrogen, where the components in air are assumed to be nitrogen and oxygen only for the simplification.

3.3.1 Conservation of Mass

The continuity equations for the gas and solids phase are given by

$$\frac{\partial}{\partial t}\left(\alpha_g \rho_g\right) + \nabla \cdot \left(\alpha_g \rho_g \vec{v}_g\right) = \dot{m} \tag{3.1}$$

$$\frac{\partial}{\partial t}\left(\alpha_s \rho_s\right) + \nabla \cdot \left(\alpha_s \rho_s \vec{v}_s\right) = 0. \tag{3.2}$$

The first term on the left in Equations (3.1) and (3.2) accounts for the rate of mass accumulation per unit volume, and the second term is the net rate of convective mass flux. The term $\dot{m}$ on right of Equation (3.1) is contributed for the gas-vapor mixture accumulation in mass from the droplet evaporation per unit volume.

The air-vapor mixture is modeled as a gas obeying the ideal gas law, which is expressed by

$$\rho_g = \frac{p_g M_w}{R T_g}, \tag{3.3}$$

where T_g is the air-vapor mixture, which can be solved by the energy equation.

3.3.2 Conservation of Momentum

Consider the interactions between droplet with gas and solids, the momentum balance equations for the gas and solids phase can be expressed by

$$\frac{\partial}{\partial t}\left(\alpha_g \rho_g \vec{v}_g\right) + \nabla \cdot \left(\alpha_g \rho_g \vec{v}_g \vec{v}_g\right) = \nabla \cdot \overline{\overline{S}}_g + \alpha_g \rho_g \vec{g} - \vec{I}_{gs} - \vec{I}_{gd} + \dot{m}\vec{v}_d \tag{3.4}$$

$$\frac{\partial}{\partial t}\left(\alpha_s \rho_s \vec{v}_s\right) + \nabla \cdot \left(\alpha_s \rho_s \vec{v}_s \vec{v}_s\right) = \nabla \cdot \overline{\overline{S}}_s + \alpha_s \rho_s \vec{g} + \vec{I}_{gs} - \vec{I}_{sd}, \tag{3.5}$$

where $\overline{\overline{S}}_g$ and $\overline{\overline{S}}_s$ are the gas and solids phase stress tensor, respectively. $\vec{I}_{gs}$ is the momentum transfer between the gas and solids phase. The source terms also include contributions not only from the vapor generation, $\dot{m}\vec{v}_d$, but also from the momentum transfer, $\vec{I}_{gd}$ and $\vec{I}_{sd}$, between droplet with gas and solids.

3.3.3 Conservation of Internal Energy

The internal energy balance for the gas phase is written in terms of the gas temperature:

$$\alpha_g \rho_g C_{pg}\left(\frac{\partial T_g}{\partial t} + \vec{v}_g \cdot \nabla T_g\right) = -\nabla \cdot \vec{q}_g - H_{gs} - H_{gd} + \dot{m} C_{pg} T_d, \tag{3.6}$$

where $\vec{q}_g$ is the gas-phase conductive heat flux, H_{gs} and H_{gd} describe gas-solids and gas-droplet inter-phase heat transfer. The last source term in Equation (3.6) accounts for the energy contribution by the droplet evaporation.

The thermal energy balance for the solids phase is given by

$$\alpha_s \rho_s C_{ps} \left(\frac{\partial T_s}{\partial t} + \vec{v}_s \cdot \nabla T_s \right) = -\nabla \cdot \vec{q}_s + H_{gs} - H_{sd}, \tag{3.7}$$

where $\vec{q}_s$ is the solids-phase conductive heat flux, and H_{sd} expresses the energy transfer between droplet and solids due to the droplet-solids collision.

3.3.4 Conservation of Species

The species conservation equation for the nitrogen component in the air-vapor mixture is

$$\frac{\partial}{\partial t}(\alpha_g \rho_g Y_n) + \nabla \cdot (\alpha_g \rho_g Y_n \vec{v}_g) = \dot{m}, \tag{3.8}$$

where Y_n is the mass fraction of nitrogen and the source term for the nitrogen species is contributed from the liquid nitrogen spray evaporation.

Equation (3.8) considers the accumulation, convection, and evaporation but neglects the diffusive flux. For the oxygen species, the mass fraction can be calculated by the species normalization equation:

$$Y_n + Y_o = 1.0 \ . \tag{3.9}$$

The above governing Equations (3.1) to (3.9) could be solved theoretically if all the items on the right side in the equations are defined. The interactions between droplet and the gas/solids phase will be given in the next section. The solids-solids momentum transfer is solved by the granular stress equation based on kinetic theory and friction flow theory [Syamlal, 1995].

3.3.5 Turbulence Model

In a turbulent particulate multi-phase flow, the particles are dispersed through turbulent flow fluctuations. The addition of particles can enhance or reduce the flow turbulence,

affecting transport behavior of both particle and flow phases. With evaporating droplet, the turbulence transport mechanism becomes more complicated. So far no literature is available to explain the three-phase turbulence modulation or two-phase turbulence with evaporations. Based on the nozzle diameter and jet velocity, the spray jet flow has a typical Reynolds number of 30,000, which means the turbulent effect should be accounted for in this phase-mixing process. In this study, a simple Prandtl mixing-length model (PMLM) was used, in which the effective fluid viscosity was modified by the characteristic turbulence length scale.

3.4 Lagrangian Approach for Droplet Phase

In this study, the droplet phase field is calculated by tracking the droplet throughout the computational domain using the Lagrangian approach. The initial distributions of droplet size and velocity in the spray could be given according to the given experimental probability density function to obtain an adequate number of discrete droplet, each of which represents a set of droplet having the same size and initial conditions. To simplify the numerical simulation, it is assumed that no droplet breakup and coalescence happen during the droplet evaporation and in the droplet penetration trajectories. However, indirect interactions among droplet are included as source terms in the gas-solids field simulation, which provides the gas/solids phase distribution of temperature, velocity and concentration.

3.4.1 Droplet Trajectories

When a droplet moves in a gas-solids flow, the forces acting on it include gravitational, gas/solids drag force, and droplet-solids collision force. To predict the droplet trajectory, one has to know these governing forces. However, there is little information available to illustrate the droplet-solids collision efficiency and momentum and heat transfer among collisions. In this model, the effective drag force for a droplet in a gas-solids flow is experienced from a particle in a fluidized bed, which will be discussed in Section 3.4.3. Then the equations of motion for each of the droplet can be written as,

$$m_{di}\frac{d\vec{v}_{di}}{dt}=\frac{1}{2}C_{di}^{*}\left|\vec{v}_{gdi}\right|\vec{v}_{gdi}\pi r_{di}^{2}+m_{di}\vec{g}, \tag{3.10}$$

where $\vec{v}_{di}$ is the instantaneous droplet velocity. C_{di}^{*} is the effective drag force coefficient for a droplet in a gas-solids media, which is based on the local relative velocity between gas and the droplet, $\vec{v}_{gdi}$.

The deterministic droplet trajectories are obtained by integrating the available velocities:

$$\frac{d\vec{x}_{di}}{dt}=\vec{v}_{di}. \tag{3.11}$$

3.4.2 Droplet Evaporation Model

Actually, the droplet evaporation will also affect droplet trajectory. Droplet evaporation will reduce droplet size and change the suspension flow field, including particle concentration, phase temperature, and phase velocities. At the same time, particle addition in the flow will also change droplet evaporation and hence droplet trajectory.

Assuming that the droplet evaporation rate depends only on the vapor concentration distribution along the radial direction from the droplet surface, we have the droplet evaporation equation as [Aggarwal *et al.*, 1984]

$$\Gamma = -4\pi\pi\rho D_d \ln\left(\frac{y_v(r_\infty)-1}{y_v(r_d)-1}\right), \tag{3.12}$$

where

$$y_v(r_d) = \frac{W_v}{W_v + W_m\left[p/(p_v(T_d))-1\right]}. \tag{3.13}$$

Equation (3.13) indicates that the surface vapor mass fraction is related to the surface temperature T_d [Chen & Pereira, 1995], a quantity obtainable from solving the heat transfer equation of a droplet as follows.

The total thermal energy required for droplet evaporation and for droplet heat-up is based on the heat transfer from the gas/solids flow. For small droplet where the Biot number is much less than unity, the heat balance of a droplet can be expressed from the lumped thermal capacity model:

$$m_d C_d \frac{dT_d}{dt} = \pi D_d Nu^* k_g (T_g - T_d) - H\dot{m}, \tag{3.14}$$

where Nu* is the effective Nusselt number for a droplet in a gas-solids mixture.

It should be pointed out that, while the droplet evaporation rate depends on the vapor diffusion, the vapor concentration on the droplet surface relies on the droplet surface temperature, which is controlled by the heat balance on the droplet. When the temperature of droplet is much less than the vapor saturation temperature, the evaporation rate is diffusion controlled, since the concentration difference across the boundary layer is small as compared to a rather large temperature difference. In this case, the heat

transferred to the droplet is used for both droplet heat-up and droplet evaporation. Once T_d is approaching the vapor saturation temperature, the droplet evaporation rate becomes heat transfer dominated. Now all the heat transferred from the gas-solids flow is used for droplet evaporation.

3.4.3 Interactions between Droplet and the Gas-Solids Phase

In the heat transfer between the droplet and the gas-solids flow, droplet-solids collision plays a very important or even dominant role. Unfortunately, there is little information available to explain the detailed collision mechanisms. Many factors may affect the collision-induced heat transfer, such as collision frequency, duration of contact per collision, and heat transfer rate during contact. When a particle approaches an evaporating droplet, it is probably in contact only for a very short period, during which there is rapid heat transfer, and after which it is pushed away by the vapor generated at the droplet surface.

However, in the numerical simulation of gas-solids flow, the momentum balance and energy balance are established, respectively, for the gas phase and solids phase. Then we need to know the amount of drag force exerted on the droplet from gas and collision contribution from droplet-particle interaction. For the gas phase, the drag force exerted on the droplet should be corrected by the gas fraction in the flow:

$$C_{D,g} = \alpha_g C_{D0}, \tag{3.15}$$

where C_{D0} is the standard drag coefficient of an isolated sphere. This equation assumes the particle is fine enough to follow the gas flow. The correction reflects the particle volume contribution in the drag force.

The heat transferred to the droplet by the gas phase can be calculated as

$$q_g = \alpha_g \pi D_d N_u^* k_g (T_g - T_d), \tag{3.16}$$

where α_g is the gas phase volume fraction in the gas-solids mixture around the droplet. The correction for the heat transfer coefficient accounts for the deduction of the convective heat transfer by the space occupied by particle in the shell around a droplet.

From Equation (3.15) and Equation (3.16), we can determine the momentum and energy transfer between a droplet and the gas phase.

3.5 Initial and Boundary Conditions

A schematic diagram of the concentric evaporating jet in a gas-solids pipe flow is shown in Figure 4.1, where the inlet flow could be separated into the jet region and ambient gas-solids flow region. In the jet flow, the fluid is the droplet-vapor mixture with low temperature, while the ambient gas-solids flow has a higher temperature as the environment with uniform solids concentration. However, numerical simulation is performed by the iterations between the Eulerian approach for the gas/solids phase and the Lagrangian approach for the droplet phase, in which the suspension flow is given by the gas-solids simulation. The initial conditions only need to be declared for the gas-solids simulation, while the boundary conditions should be given for both gas-solids flow and droplet phase calculation.

3.5.1 Initial Conditions

The initial values of all field variables for the gas and solids phase must be specified for the entire computational domain, including gas volume fraction; gas pressure;

temperature for both gas and solids; velocity for both gas and solids; and species mass fraction for nitrogen and oxygen. The initial conditions need to be accurate enough to allow convergence. The initial conditions can also be given by a pre-calculated numerical simulation result. For example, the initial velocity distribution is given by a calculation with a specified inlet velocity. For the droplet trajectory calculation, the suspension gas-solids flow is given by the two-fluid Eulerian approach. No initial conditions are required, and the computational domain is also given by the gas-solids suspension flow.

3.5.2 Inlet Boundary Conditions

An inflow boundary condition should be specified at the inlet position, where all the field variables need to be specified. In this study, the inflow includes the inlet jet flow and concurrent gas-solids flow, which are specified in the jet region and inlet gas-ambient flow region, respectively. The gas and solids phase inflow conditions are given in the gas-solids flow simulation section, while the droplet inflow conditions are given in the droplet trajectory starting positions.

The inflow boundary conditions for gas-solids in the jet region are given by

$$\begin{cases} V_{gi} = V_{gj} \\ T_{gi} = T_{gj} \\ \alpha_{gi} = 1.0 \\ Y_n = 1.0 \end{cases}, \tag{3.17}$$

where V_{gj} and T_{gj} are the initial jet velocity and the temperature of vapor in the vapor-droplet mixture, respectively. In this study, the initial gas jet velocity is assumed to have the same velocity as the droplet, which is calibrated by the LDV method. The initial vapor may have the same temperature as the droplet saturation temperature at standard air

pressure. However, near the nozzle region, the entrainment and fluctuation is very severe. In this study, we specified a vapor temperature of 150 K, which is higher than the droplet temperature. Since the initial solids volume fraction is zero in the jet region, the solids velocity and solids temperature are not required. The only component in the gas phase in the jet flow is nitrogen, a unit species mass fraction is given as the initial jet condition.

The inflow boundary conditions for the gas-solids phase in the jet ambient flow are given by

$$\begin{cases} V_{gi} = V_{ga0} \\ V_{si} = V_{sa0} \\ T_{gi} = T_{ga0} \\ T_{si} = T_{sa0} \\ \alpha_{gi} = \alpha_{ga0} \\ Y_n = 0.7 \end{cases}, \tag{3.18}$$

where both velocity and temperature of gas and solids phase should be given since the initial gas volume fraction is not unity. Also, the initial nitrogen species mass fraction is given as 0.7.

As discussed before, the evaporating spray is treated using the Lagrangian trajectory approach, in which the droplet consist of a finite number of trajectory groups. Each droplet initially starts out with a known position, velocity, size and temperature, which are dependent on the spray jet system characteristics. So, the inflow conditions for the droplet trajectory calculation include the distribution of droplet size, velocity, and number density. In this study, a uniform droplet and uniform number density distribution is given in the nozzle region.

3.5.3 Outlet Boundary Conditions

In this study, the pressure at the outflow boundary is assumed to be constant. In the gas-solids flow simulation, it is given as

$$P_g\big|_{exit} = P_{stat} = 1.01\times10^5 \ Pa. \tag{3.19}$$

3.6 Numerical Solution Procedure

In this study, the gas-solids suspension flow was simulated using the Eulerian two-fluid model. The source terms appearing in the mass, momentum, and energy equations represent the interactions between droplet and the gas/solids phase. In all the calculations performed within the droplet evaporation and trajectory model, the distributions of velocity, temperature, and concentration of gas and solids are given as a function of the spatial position at an instance of time. This snapshot of the continuum fields is obtained from the gas-solids flow simulation and is fixed during the calculation of droplet trajectories. The overall source terms for the gas-solids simulation are accumulated, which include the vapor mass, drag force on gas and solids phase, and heat transfer from the gas and solids phase. The average droplet temperature in each control volume is also needed to estimate the source term for the gas phase energy equation due to droplet evaporation.

The solution procedure for the evaporating spray jet in gas-solids flows was performed by the Multiphase Flow with Interphase eXchange (MFIX) code and droplet evaporation mode code, which was self-developed with Argonne National Laboratory. The flow chart of the solution procedure is shown as Figure 3.1, where the droplet trajectory model is called with a time interval defined by the user. At the beginning of

each time step, all the explicit quantities are calculated. Then the difference equations are solved sequentially within the iteration loops. The cells are visited one at a time starting from the cell with the lowest index and going to the cell with the largest index. Convergence is said to occur when all the discredited equations are satisfied simultaneously in all the cells without having to make adjustments in any of the cells.

The solution starts with a guessed pressure field. Initially the gas continuity equation is checked to see if it is satisfied. If not, the pressure is adjusted using Newton's method. If the energy or the species balance equations need to be solved, they are solved for temperature and species mass fractions. The fluid density is updated. The coupled fluid and solids momentum equations are solved for the velocity components. The solids continuity equations are then solved for the solids volume fraction. The gas volume fraction is then calculated by subtracting the solids volume fraction from one. The above steps complete one pass of the inner iteration for a cell. The inner iterations are continued until the fluid continuity equation is satisfied or the number of inner iterations exceeds a specified limit, which is defined as five.

The inner iterations are continued for all the numerical cells to complete one pass of the outer iteration. The outer iterations are continued until the solution reaches the point at which no further inner iterations are needed, which implies that the existing solution satisfies all the discretized equations simultaneously in all cells. When such a convergence is obtained or when the number of outer iterations exceeds a specified limit, which is defined as 50 in this solution, the calculations proceed to the next time step. If the time interval for the droplet trajectory calculations is reached, the droplet evaporation

model will be called, which provides the updated source items representing the interactions between droplet and the gas/solids phase.

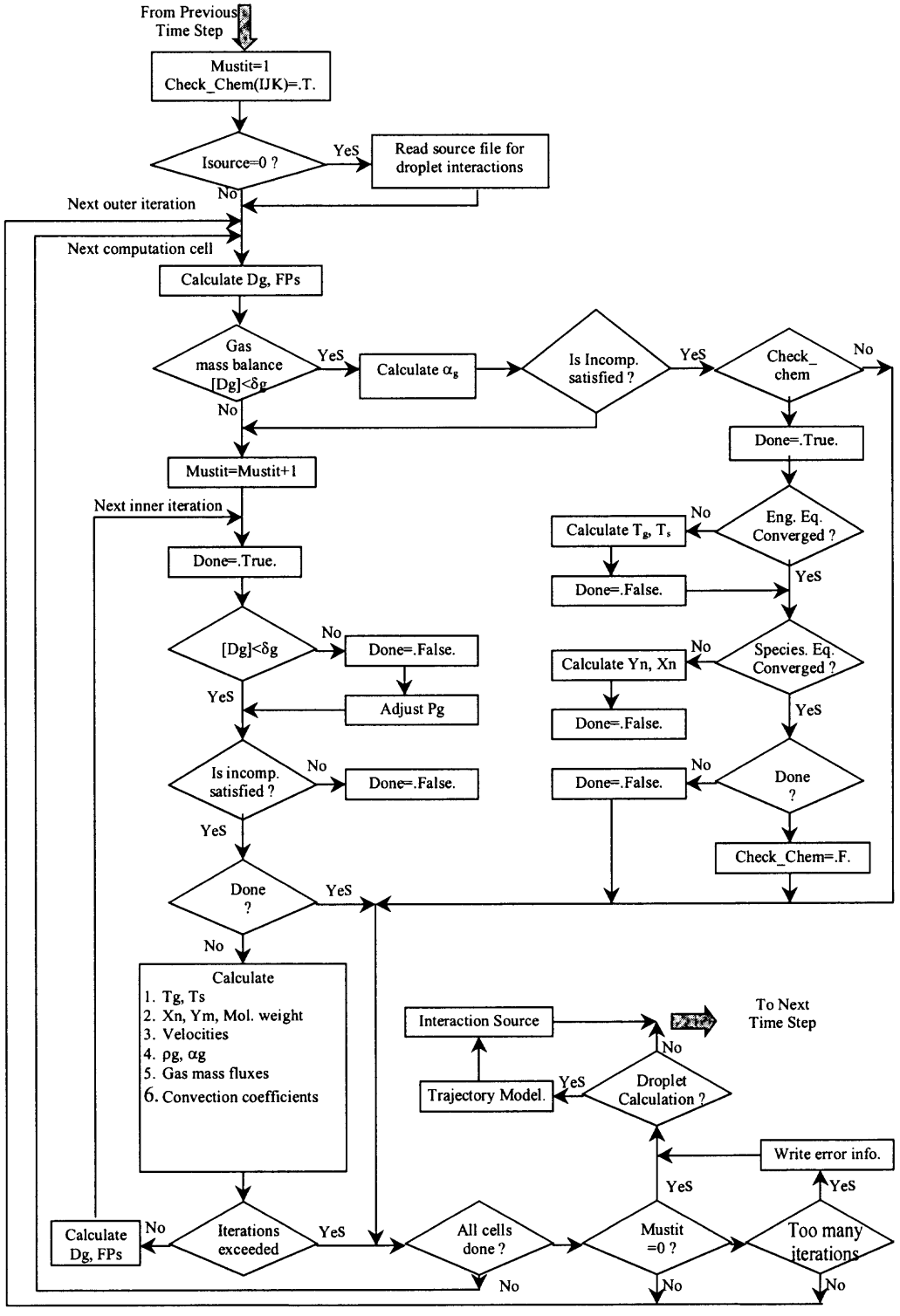

Figure 3.1 Flow chart of the numerical simulation procedure.

3.6.1 Initial Gas-Solids Flow Field

To achieve a convergent multi-phase flow solution with strong inter-phase exchange, a good initial gas-solids flow is the first step toward success. In this study, the initial gas-solids flow field represents the initial field without the droplet evaporation source terms, while the complex inlet boundary conditions are incorporated near the nozzle region, such as velocity difference, temperature difference, and solids concentration difference between the flow in the nozzle and the ambient gas-solids flow. The typical inlet conditions in the nozzle include a velocity of 35 m/s, temperature of 100K, solids concentration of 0 (solids free). However, the ambient gas-solids inlet flow has a velocity of 3 m/s, environmental temperature of 300K, and a concentration of 5%. Combining all these factors often results in divergence of the solution.

In this study, the procedure was separated into many sub-steps. For example, we tried to achieve the gas-solids field with uniform inlet conditions as the first step. This solution represents the flow field with the effect of the other boundary conditions, for example the boundary of the wall. In the next step, we increased the flow velocity in the nozzle region. The obvious velocity difference between the flow in the nozzle region and the ambient flow quickly changes the distribution of the flow field velocity and concentration. This solution represents a typical two-phase jet flow with the same temperature. Because of the low temperature of liquid nitrogen in the spray jet, the temperature of the vapor is very low compared with that of the ambient flow. Based on same temperature two-phase jet flow, we reduced the temperature of jet, resulting in a solution for a two-phase jet with temperature difference. Finally, the solids concentration condition is released, which represent a low-temperature gas jet inserted into a high-

temperature gas-solids media. Some typical results illustrate the effect of solids concentration, jet velocity and temperature on the phase mixing.

By the end of the initial gas-solids field simulation, the data file, with a full description of phase distributions of velocity, temperature, and concentration will be outputted for the droplet trajectory calculation.

3.6.2 Droplet Trajectories in Gas-Solids Suspension Flows

The evaporating spray is treated using the Lagrangian trajectory approach, in which the droplet consist of a finite number of trajectory groups. Each droplet starts out with a known position, velocity, size, and temperature, which are dependent on the spray jet system characteristics. The overall droplet position and velocity are updated over the time step, depending on the interactions between the droplet and local gas-solids flow, which is given by the gas-solids flow simulation. The solution flow chart of the trajectory model is shown as Figure 3.2. The detailed procedure is described in the following.

The solution starts from a given droplet location, size, and velocity. Based on this location in the calculation domain, the local values in velocity, temperature, and volume fraction of gas and solids can be interpolated. Each integration step along the trajectory starts with an update of thermodynamic and transportation properties of the gas and liquid phases. Then the Nusselt number for heat transfer and drag force coefficient are calculated, taking into consideration the local concentration of the solid particles. The integration time step is estimated from the droplet velocity and grid dimension. A minimum of 10 points is required within one mesh distance. From Eq. (3.11) the new droplet location can be determined from the local droplet velocity and the time step.

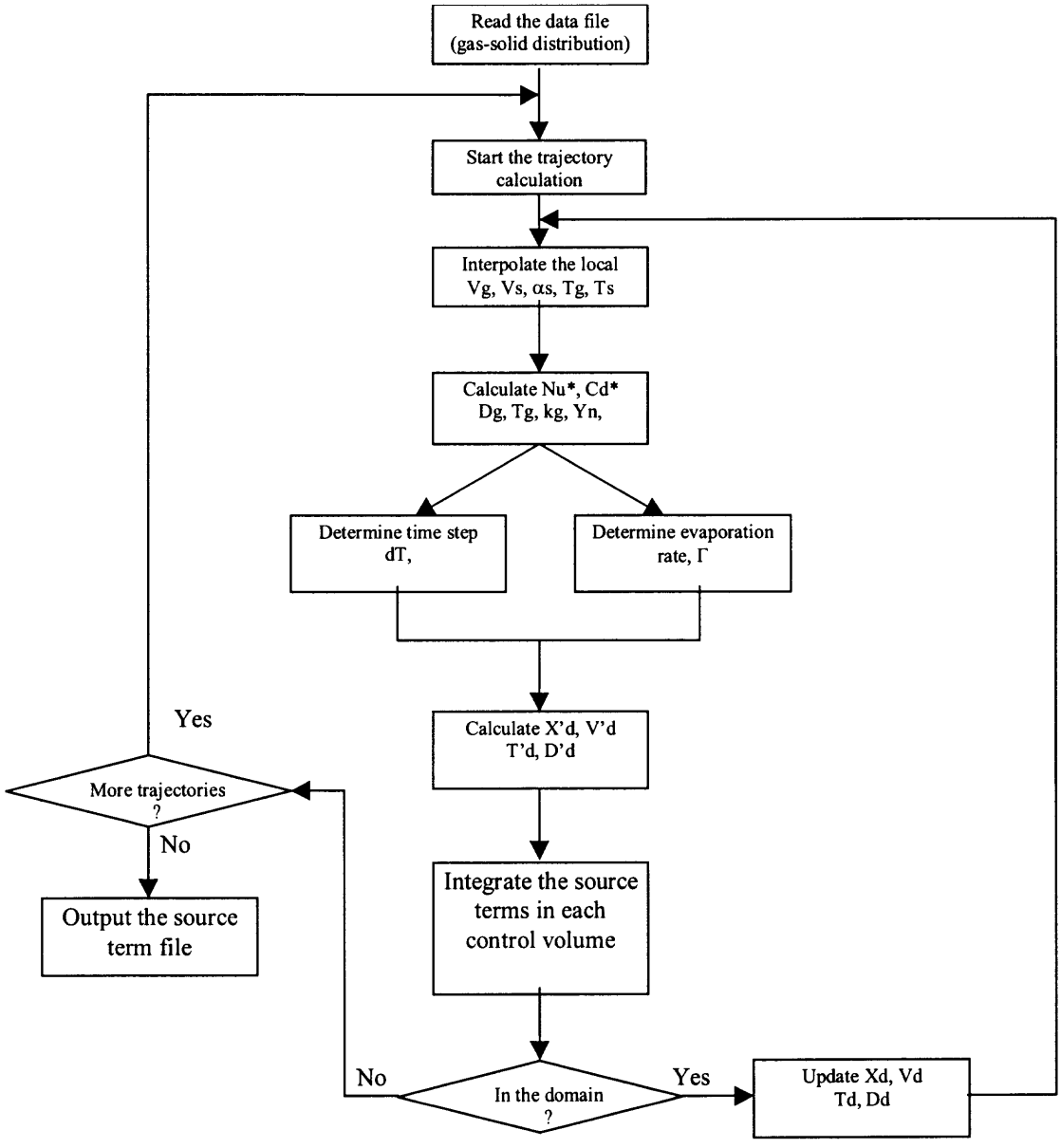

Figure 3.2 Flow chart of droplet trajectory calculations.

The droplet velocity, droplet size, and droplet temperature are updated from the droplet mass, momentum, and energy conservation equations. This time integration is continued until the droplet is totally evaporated. In this calculation, this criterion is

established as a droplet diameter of less than 5 μm. The entire droplet trajectory calculation is then repeated for a range of different droplet initial conditions representing the nozzle characteristics.

The droplet trajectory model must calculate the source terms for use in the continuum phase calculations. These calculations establish the interactions between droplet and gas and solids phase, respectively, which include the droplet evaporation rate, momentum, and heat transfer. These source terms are volume averaged for the cumulative results over all the trajectory calculations. The updated gas-solids flow fields are used in the next iteration over the droplet trajectory calculations. For reasonable computational speed, the calculation of trajectories cannot be done at every time step within the gas-solids flow code. Usually, the trajectories are updated every four to eight time intervals depending on the simulation domain and the complexity of the flow field.

3.6.3 Gas-Solids Flow Field with Source Terms

The gas-solids flow field with droplet evaporation is further simulated, incorporating the source terms from the droplet trajectory calculations. The typical effects of droplet evaporation include the dilution of solids concentration, reduction of phase temperature, and change of the phase velocity. Many factors will affect the gas-solids flow field, which depends on the spray jet mass flow rate and droplet evaporation rate. These strong interactions sometimes even affect the calculation convergence, due to the huge amount of vapor generation. As a better solution, the computation is initially performed with a low liquid mass flow rate to avoid the divergence, then with a higher liquid flow rate.

By repeating this procedure, the convergent solutions of gas-solids-droplet flow can be achieved. The interactions among the phases are also realized, which provides an explanation of some of the experimental phenomena and a better understanding of the mixing process of evaporating spray jet in gas-solids flows.

CHAPTER 4

EXPERIMENTAL METHOD

4.1 Introduction and Experimental Setup

General characteristics of three phase flow with sprays from rectangular nozzles in circulating fluidized bed were investigated. The effects of various solid loadings and orientation angle effect of rectangular nozzle are also studied. For the second objective, the spray jet expansion and the effect of jet-jet interaction are investigated experimentally for evaporating liquid nitrogen spray jets in dilute air –FCC cross-flows. The expansion behavior as well as spray trajectories and deflections were determined from the temperature field measurements using thermocouple matrix module. For these experimental purposes, specially designed arc-shape eight feet height chamber was developed and equipped with thermocouple matrix module to get the temperature field information.

4.2 Circulating Fluidized Bed Loop

In order to investigate the liquid spray jets in gas-solid flows, an arc-shaped circulating fluidized bed (CFB) system, as shown in Figure 4.1, was built to simulate jet expansion, deflection and jet-jet interaction in a continuous gas-solid flow. The major parts of the CFB include a riser, a cyclone separator, a down comer, and an induced fan. All of the experiments were carried out in the CFB riser, which has pi-shaped cross-section, which has 10 inches width and 8 feet height channel made of transparent plastic material.

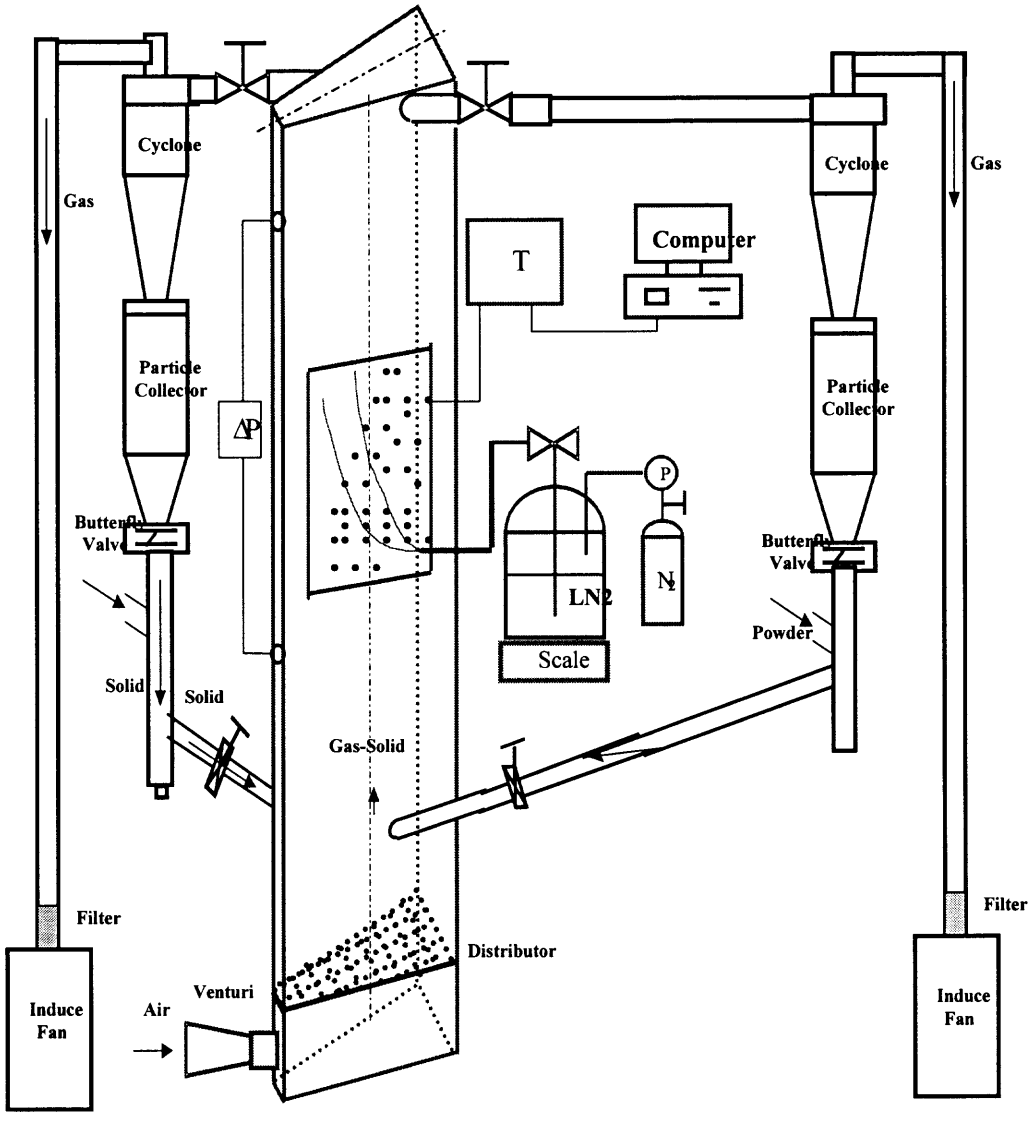

Figure 4.1 Schematic diagram of experimental system.

The high collection efficiency cyclone (6″ I.D., PE-06, RSG) was used to separate and collect solid particles from gas-solid flows that come from the CFB riser. We replaced conventional metal distributor to new mesh type distributor to reduce pressure drop. The fluidizing gas is introduced into the system through a stainless steel sieve gas

distributor located at the bottom of the riser. The distributor with an average pore size of 20 micron can provide homogeneous gas distribution over the whole bottom of the bed and protect the leakage of solid particles. Dual Cyclone-Standpipe enables system in increase gas flow rate. The fine particle laden gas from the cyclone exit is further filtered through the vacuum filter of the induced fan before it is discharged to the building ventilation system. Since the pressure inside the loop is kept lower than that of the ambient air, there is no out-leaking particulate pollution. Feed of solid particles into the riser is crucial in the experiments and needs special precaution, as controllable particle feed rate need to be achieved. Dual spray feeding System was adapted to stabilize the particle feeding. A continuous system has been developed to feed a recycled amount particles.

(a) CFB chamber (b) Mesh distributor and glass bead inlet (c) Dual cyclone

Figure 4.2 CFB parts.

The feeding system includes a particle container which collects the particles from the cyclone, a butterfly valve, located under the container, which is used to shut off the

supply of particle to down comer pipes, as well as one part of devices to measure the solid volume fraction, and a ball valve near the feed inlet, which functions as a feed control valve to adjust the particle flow rate. The particles are fed into the riser 15 cm above the distributor and carried upward by the fluidizing gas. The solid particles are, then, separated in the cyclone and fed again into the riser to generate a continuous gas-solid flow.

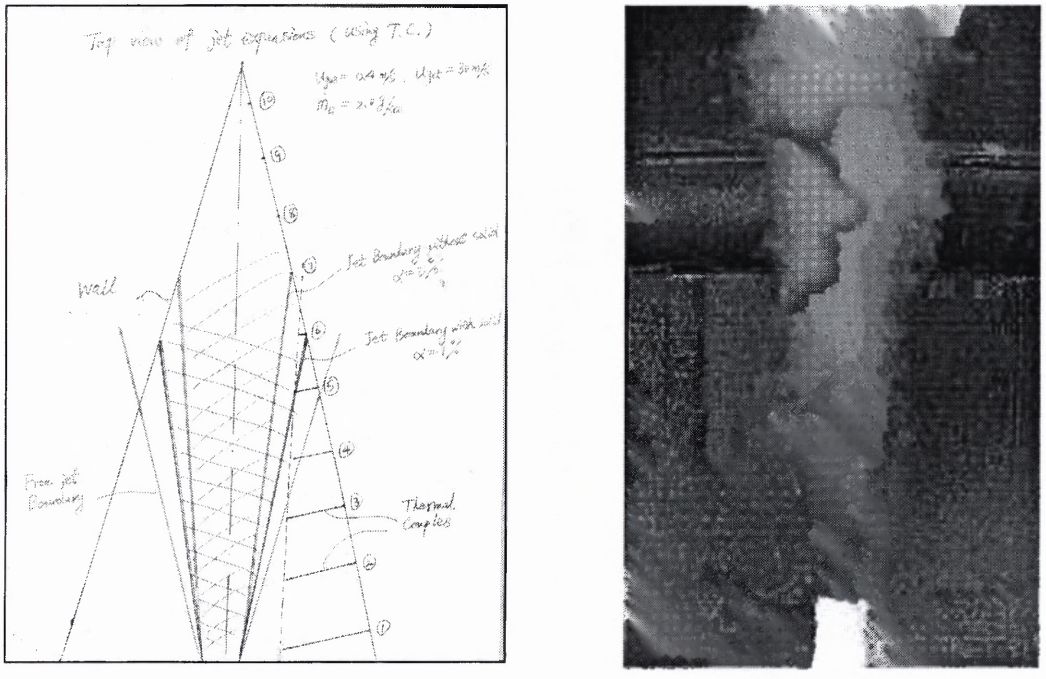

(a) Schematic jet trajectory in confined chamber (b) Picture of flat nozzle free jet

Figure 4.3 Illustration of jet trajectory and actual jet.

The solid particle used in the fluidized bed is FCC particles with a bulk density of 1250 kg/m^3 and the average particle size of 70 micron, calibrated by AeroSizer. New wall structure was applied for test-section to reduce electrostatic effects and to prevent

wall cracking from extremely cold spray jet contact. To prevent electrostatic charging in the fluidized bed, the whole setup is grounded. Moreover, in all regular tests Larostat 519 (dimethylethyl ammonium ethosulfate supported on silica, PPG/Mazer Chemicals, kindly supplied by ExxonMobil) as anti-static agent has been used. Due to the small particle size of the powder, some anti-static agent leaves the solid particle circulation loop. In order to remain the anti-static effect, a small amount of Larostat should be regularly added into the system. The test section is located at 1.2 meter above the distributor, where a fully developed gas-solid suspension is achieved.

4.3 Liquid Nitrogen Spray-Jet System

We examined LN2 spray jets in cross-flow air–FCC suspension streams under the room conditions. Effects of different particle loadings on the jet penetration as well as jet deflections were investigated. Here are the nozzle diagram and the dimensions of each nozzle.

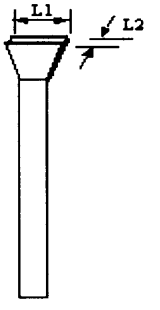

Figure 4.4 Schematic diagram of nozzle.

Table 4.1 Nozzle specifications.

Nozzle number	Nozzle-1	Nozzle-2	etc
Openness (mm)	2.8x1.0	3.8x1.0	(L1×L2)
Nozzle type	Flat		
Length (mm)	150		

4.3.1 Velocity Measurement

The droplet velocity at the exit of nozzles has been calibrated using a Laser Doppler Velocimetry (LDA) measurement system (1-D FlowLite w/BSA F60, with 10 mW He-Ne Laser, DANTEC).

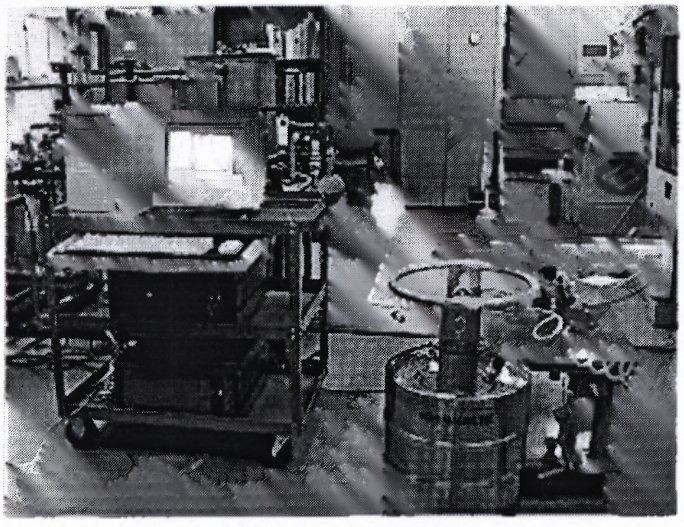

Figure 4.5 LDV system.

Figure 4.5 gives the histogram of velocity distribution of the flat with 20,000 sampling points, which indicates that the velocities are Gaussian distributed. The averaged velocity is about 24 m/s with 7.5 m/s in standard deviation for the exit velocity.

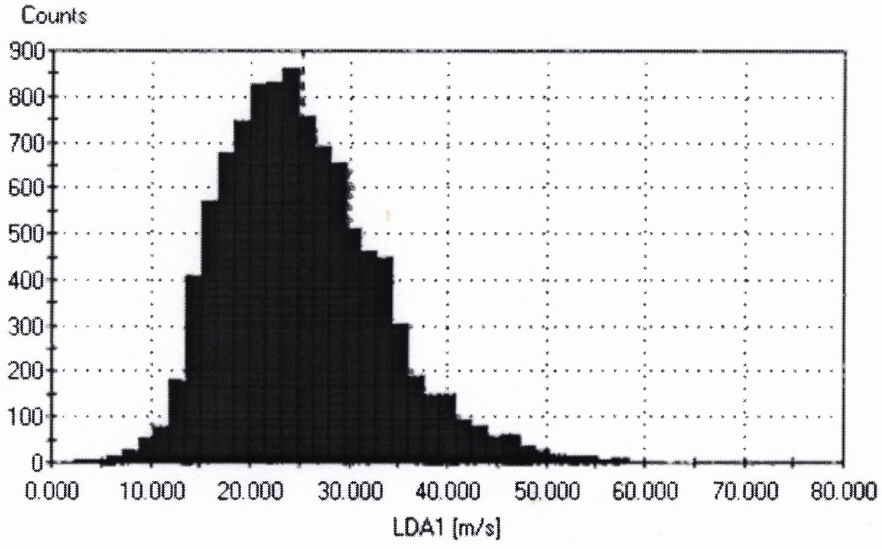

Figure 4.6 Velocity distribution of flat nozzle.

Under the assumption of no velocity slip between the vapor and droplet at the nozzle exit, the vapor volume fraction in the initial vapor-liquid mixture could be estimated from liquid mass flow rate and droplet velocity by

$$\alpha_g = \frac{1}{\rho_d - \rho_g}\left(\rho_d - \frac{M_j}{\pi r_j^2 v_d}\right) \qquad \textbf{(3.2)}$$

4.3.2 Pressure-controlled Spray System

As mentioned in the foregoing section, the disadvantage of self-controlled spray system is the instability of mass flow rate combined with injecting velocity. Moreover, the tank capacity of 5 liters is not large enough to keep running the experiment for a needed time at a higher mass flow rate. Therefore a more accurate spray system, the pressure-controlled spray system with 25 liters capacity, as shown in Figure 4.7, was developed and utilized in most of this study. The stable pressure cylinder tank can keep a constant

pressure in the liquid nitrogen container and results in a stable spray jetting velocity. In addition, the spray mass flow rate can be adjusted by regulating the container pressure.

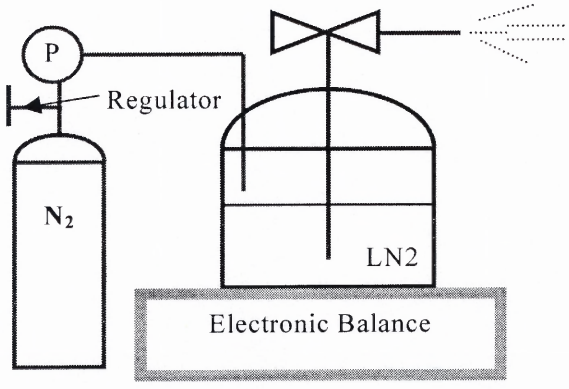

Figure 4.7 Schematic diagram of pressure-controlled spray system.

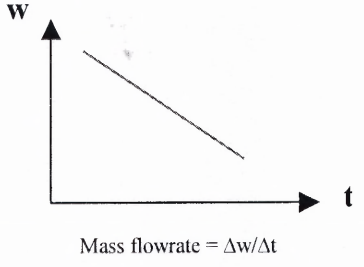

Figure 4.8 Mass flow rate of pressure-controlled system.

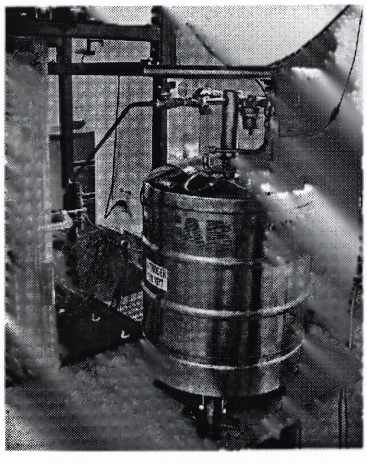

Figure4.9 Pressure-controlled spray system.

Calibration of nozzles with pressure-controlled spray system was also performed using the Laser Doppler Anemometry (LDA) measurement system. The mass flow rate, mean velocity, standard deviation, and liquid volume fraction are listed in Table 4.2.

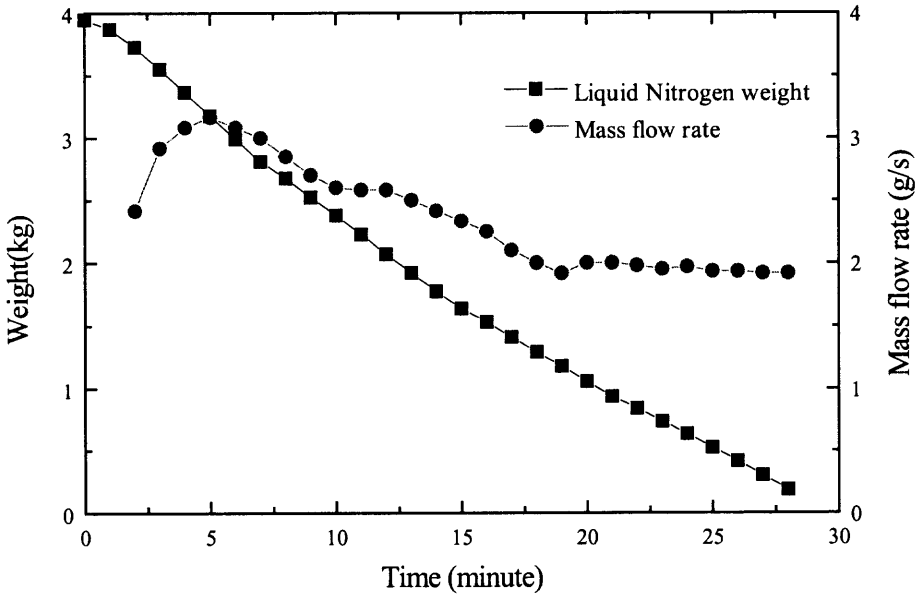

Figure 4.10 Calibration of mass flow rate of flat nozzle.

Table 4.2 Calibration of Flat nozzle.

Nozzle	Mass flow rate (g/s)	Mean Velocity	σ (m/s)	Liquid volume fraction (%)
Flat	2.33	24	7.5	5

4.4 Thermocouple Matrix Module

Expanded Thermocouple Matrix module which has 16 thermocouples has been developed to study jet deflection and to define local spray boundary. Figure 4.11 shows the general system diagram and Figure 4.12 , Figure 4.13 illustrate the mechanism of the measurement system. 16 thermocouples (HTMQSS-020U-6, Omega) are connected with

a 24-switch device (TOGGLE SWITCH, GRAINGER). The switch box is connected to isolated data acquisition system (OMB-MultiScan-1200, Omega), which has 24 channels and maximum 8000 Hz sampling frequency, and control which group is measured.

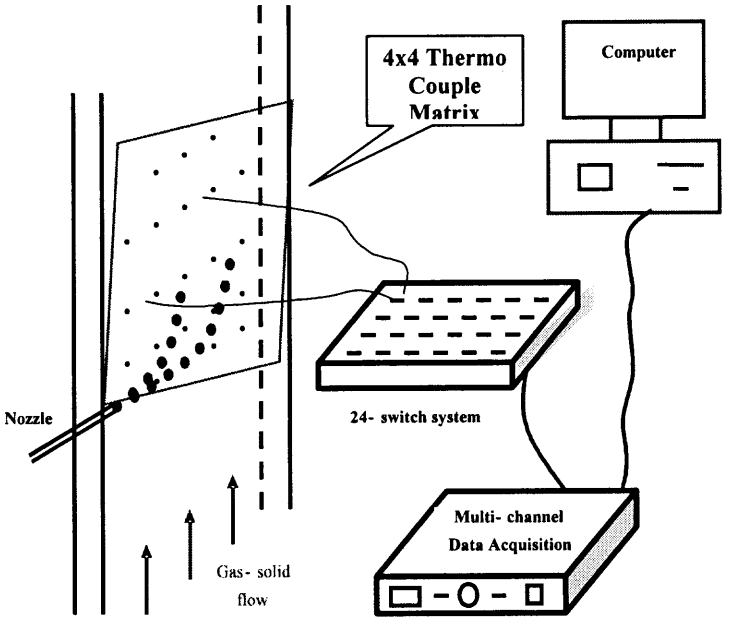

Figure 4.11 Temperature measurement system.

Pentium III computer with ChartView32 (Omega) is used to connect with the data acquisition system and get the temperatures real time. In the experiments, the sampling time is 25 seconds and the sampling frequency is 4 Hz or 8 Hz. Figure 4.13 shows a typical distribution of thermocouples. In order to prevent thermocouples from picking up static charges, all thermocouples are ungrounded by connecting to a tap water pipe.

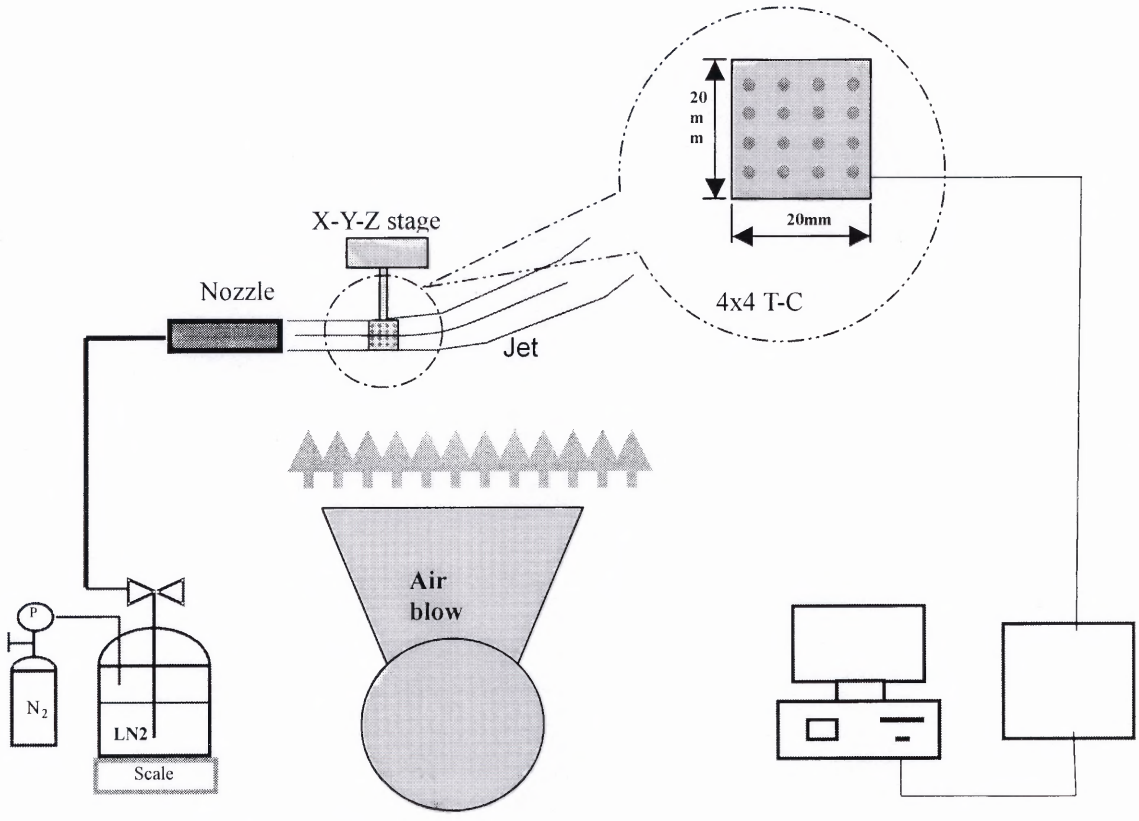

Figure 4.12 Diagram of thermocouple matrix module.

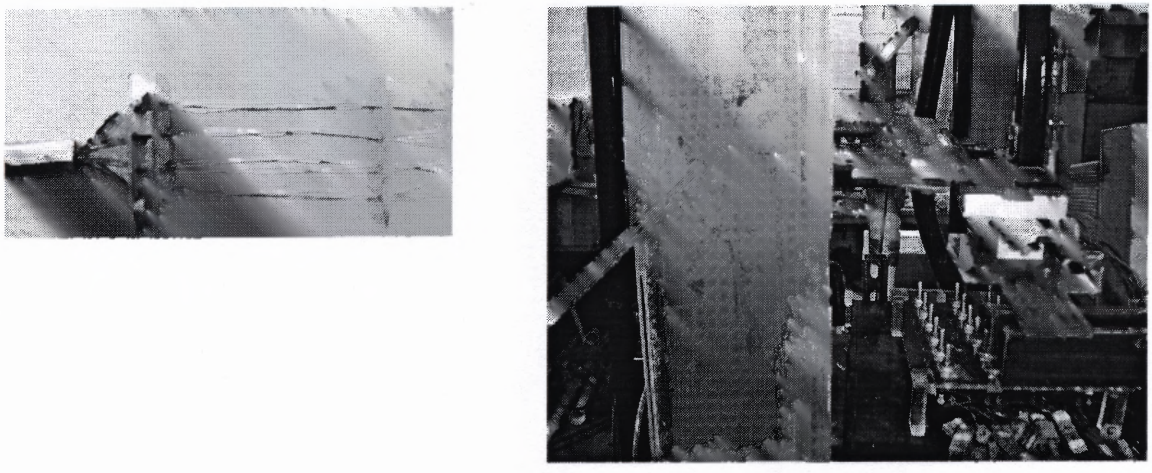

(a) Thermocouple module

(b) System attached with T-C module

Figure 4.13 Picture of thermocouple module and the system with t-c module.

Determination of experimental parameters and ranges

To illustrate the various parametric effects, in this study, the jet flow rate ranges from 0.2 to 0.5 (lb/min). Spray penetrations in suspensions with different solid volume fractions (0%, 1.0%, 1.5 %) were also investigated. The spray jet velocity is from 20 to 35 (m/s). The CFB is operated at the room temperature. The spray liquid is liquid nitrogen.

Verification of T-C module on free jet in cross-flow

Operation conditions

- Room Temp. T =76°F
- Nozzle: flat(0,2 mm slot, 10mm long)
- Droplet pushing Pressure: Pair = 20psi
- Air blower velocity : V = 1.5m/s

Results

Mini-T.C. probe module can accurately detect spray boundary and even deflection

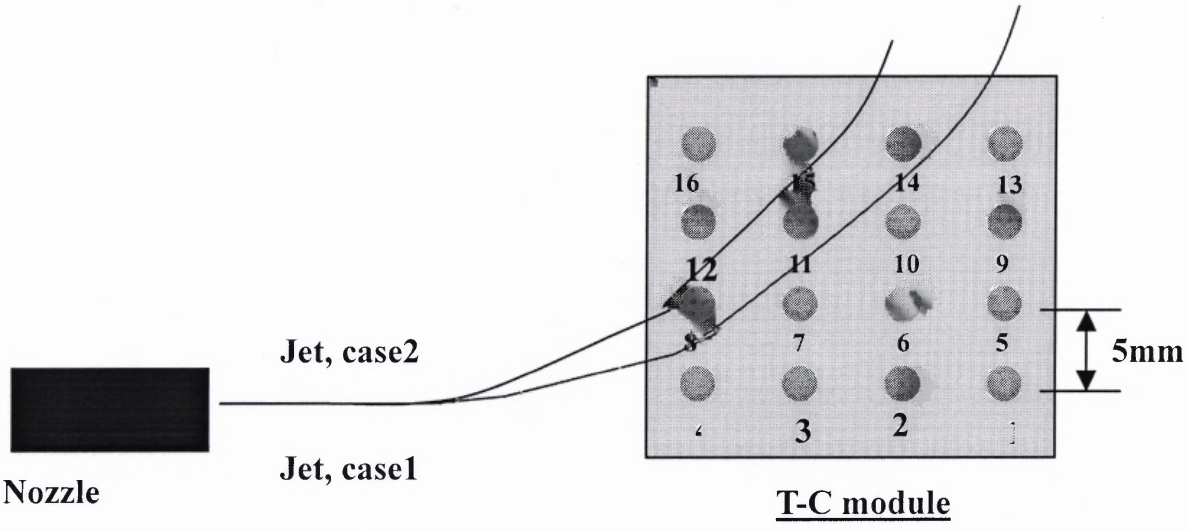

Figure 4.14 Cross-flow free jet trajectory.

Table 4.3 Temperature measurement distribution.

T-C number	1	2	3	4	5	6	7	8	9	10	11	12	13	14	15	16
Case 1, Temp.	5	-4	-31	-64	4	-17	-88	-115	-17	-54	-127	-30	-22	-86	-85	-5
Case 2, Temp.	34	23	5	-11	26	5	-7	-66	21	12	-7	-128	18	0	-149	-136

Using this T-C module, the trajectory of droplet evaporation for the local area was obtained. Therefore T-C matrix is used for whole picture and tendency of jet trajectory.

CHAPTER 5

RESULTS AND DISCUSSION

5.1 Computational Domain and Flow Conditions

Numerical simulation has been performed for a cross-flow liquid nitrogen spray from a rectangular nozzle with a fan angle that is injected into a fully developed gas-solid flow in a circulating fluidized bed with a rectangular cross-section.

5.1.1 Geometry

For the convenience of experimental comparison, a liquid nitrogen spray jet in an air-FCC flow is simulated under conditions similar to the experiments in (Liu, 2003). The computational domain is selected to be 30 cm ×10 cm × 2.5 cm. Calculation domain is illustrated in Figure 5.1.

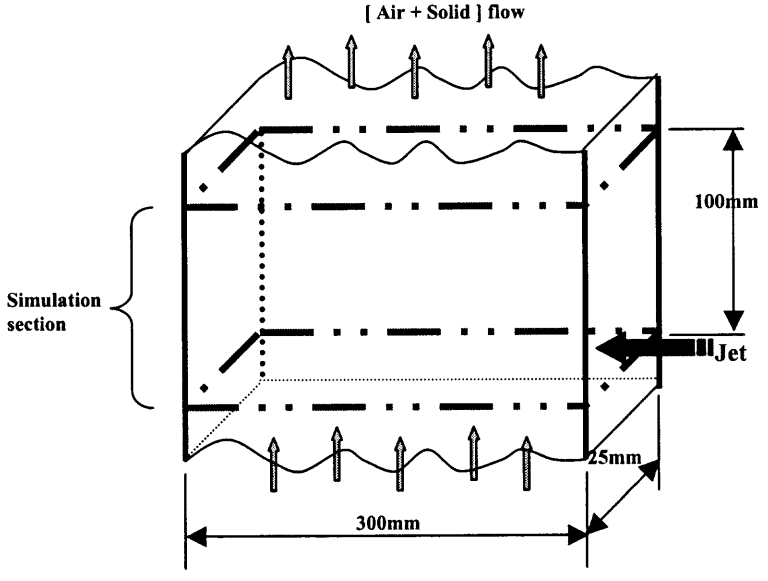

Figure 5.1 Computational domain geometry.

5.1.2 Operation Conditions and Material Properties

The flow conditions are listed in Table 5.1. These cases are the standard cases carefully selected for parametric studies with following reasons. 0% case is needed for comparison of with solid and without solid. Due to the limit of lab scaled experiment, the maximum solid loading is up to 1.5 %. For code verification, 1% case is needed. For extended study with large amount of solid loading, 15% and 25% cases are selected, which is practically used in industry. 5% solid loading with horizontal and vertical nozzle orientation also have been performed but it is not list in the table. Because significant characteristic changes occurs in between non-solid and with solid loading as explained in later chapter, therefore the 5% case is not necessary for parametric study and only used for number sensitivity in the next section.

Table 5.1 Calculation conditions.

Case No.	1	2	3	4	5	6	7	8	9	10	11	12	13	14	15	16
Aspect ratio	1:3	1:4	1:3	1:4	1:3	1:4	1:3	1:4	1:3	1:4	1:3	1:4	1:3	1:4	1:3	1:4
Solid volume fraction(%)	0%		1%		15%		25%		0%		1%		15%		25%	
Solid velocity(m/s)	0				3				0				3			
Nozzle orientation	Horizontal								vertical							
Gas velocity(m/s)	3															
Spray velocity(m/s)	35															
Initial gas temp(K)	300															
Initial solid temp(K)	300															
Gas temp at nozzle(K)	100															
Gas pressure(Pa)	101,300															
No-slip conditions.	No-slip conditions. Velocity vanish at the wall															

Table 5.2 Material properties of three-phases.

phase	Properties	values
Gas	Specified constant gas viscosity	1.8E-5 N.s/m^2
	Average molecular weight of gas	29
Solid	Particle density	1200 Kg/m^3
	Particle diameter	70 μm
	Particle elasticity	0.9
	Packed bed void fraction	0.4
Droplet	Droplet temperature at nozzle	60 °K
	Droplet mass flow rate	1.2 g/sec
	Droplet diameter at nozzle	160 μm

Material : 3-phases ; Gas(air) / Solid(FCC) / Droplet (liquid nitrogen)

5.1.3 Mesh Generation and Number Sensitivity

In order to test grid sensitivity, two different meshes with uniform grid distributions are selected for the same calculation geometry, one with 30×20×20 mesh and the other with 60×40×25 mesh, as indicated in Figure 5.2. Except the solid loading of 5%, all other

operating conditions are listed in calculations table. The droplet size (d_{32}) distributions with these two sets of meshes are shown in Figure 5.3. As a test variable, the spray evaporation length (defined as the droplet maximum penetration in the original spray jet direction) has been used to monitor the simulation convergence, which strongly depends on the suspension flow fields.

Figure 5.3 indicates that calculation result is not very sensitive to the computational mesh density. The spray evaporation length is 25 cm with a uniform mesh of 20 × 20 × 30 and 23 cm with a uniform mesh of 25×40×60. The difference is about 8%, which is tolerable, especially for the purpose of mechanistic and parametric study. In this study, to achieve the same degree of convergence, the computational time using the grid of 25×40×60 meshes is at least one order of magnitude longer than that using the grid of 30×20×20 meshes, depending on spray and flow conditions. Hence, to save the computational time, the grid of 30×20×20 meshes is used in the rest of this study. Furthermore, to get the phase distributions within the spray region, a variable mesh with the same total number of grids is adopted in this study, as shown in Figure 5.2(c).

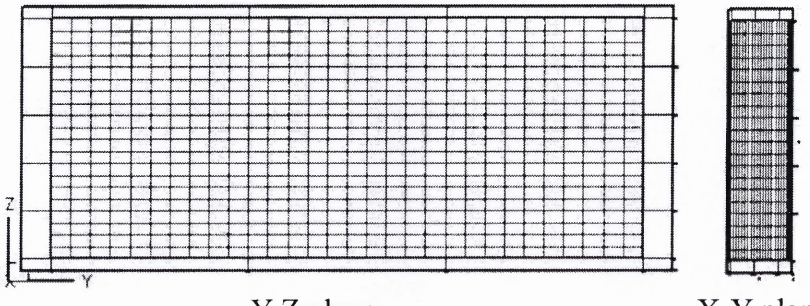

Y-Z plane X-Y plane

(a) 20 x 20 x 30

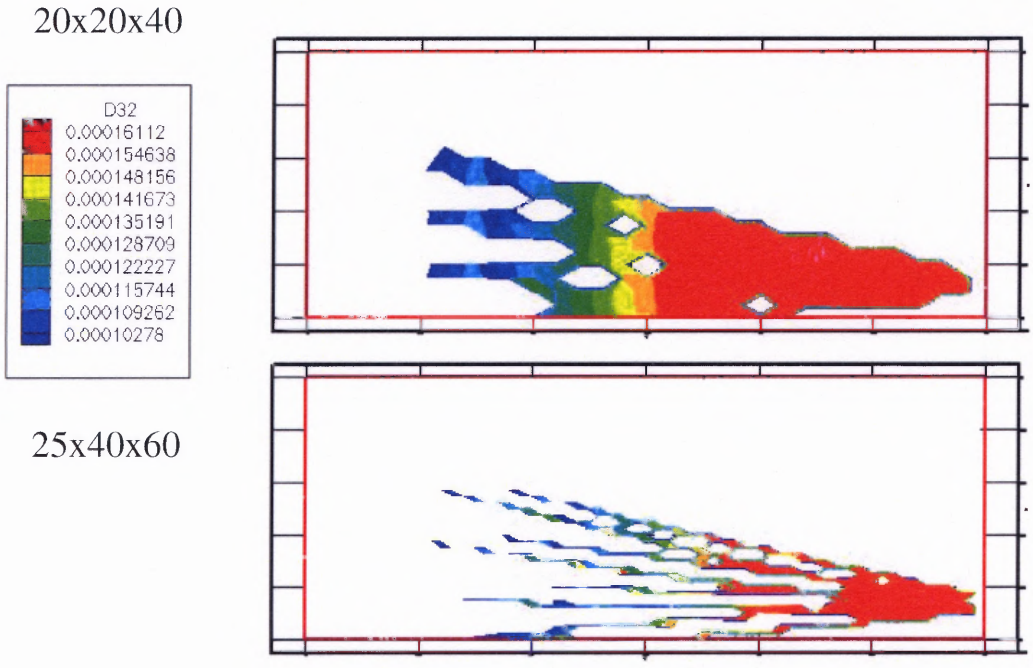

Figure 5.3 Effect of grid sensitivity on spray structure (5% solids volume fraction).

5.2 Comparison with Measurement and Code Validation

Code verification for co-current spray with round nozzles (2-D axial-symmetric flows) was carried-out by Wang (2002). In this study, code verification for cross-flow spray with rectangular nozzles has performed at different aspect ratio and orientations (3-D flows).

Following table is a operation conditions for the experiment and the same condition was applied for numerical simulations as list in the table with case number 3,4, 11 and 12. Figure 5.4 (a) demonstrates the jet trajectory determined using the 48-thermocouple matrix system. The jet penetration length here is defined as the horizontal distance from the nozzle exit to the point where the jet droplet are completely evaporated

5.2 Comparison with Measurement and Code Validation

Code verification for co-current spray with round nozzles (2-D axial-symmetric flows) was carried-out by Wang (2002). In this study, code verification for cross-flow spray with rectangular nozzles has performed at different aspect ratio and orientations (3-D flows).

Following table is a operation conditions for the experiment and the same condition was applied for numerical simulations as list in the table with case number 3,4, 11 and 12. Figure 5.4 (a) demonstrates the jet trajectory determined using the 48-thermocouple matrix system. The jet penetration length here is defined as the horizontal distance from the nozzle exit to the point where the jet droplet are completely evaporated along its trajectory where as the jet deflection is defined as the vertical distance of the same two points described above.

Table 5.8 Experiment operation conditions.

	Case No.			
Case Number	1	2	3	4
Nozzle orientation	Nozzle-1 Vertical	Nozzle-1 Horizontal	Nozzle-2 Vertical	Nozzle-2 Horizontal
Aspect ratio a/b	2.8	2.8	3.8	3.8
Hydraulic diameter (mm)	1.26	1.26	1.47	1.47
Jet velocity(m/sec)	25	25	20	20

Ambient velocity(m/sec)	0.41	0.41	0.41	0.41
Volume fraction (%)	1.5	1.5	1.5	1.5
Jet flow rate (lb/min)	0.45	0.45	0.4	0.41

The centerline of the spray jet is plotted just below the points of minimum temperatures at the thermocouple grid. This interpretation is based on the fact that the evaporation rate of the liquid spray in the downstream is less than that in the upstream due to the reduced interaction between the spray and the fluidized gas-solid medium. In addition, the smaller droplet tend to migrate to the wake region of the jet that may further deviate the true centerline of the jet towards a location slightly upstream to where the minimum temperature is found.

Effect of nozzle orientation, as shown in Figure 5.4 (a), can be best illustrated from the comparison of the penetration between the vertical orientation and the horizontal orientation of the same rectangular nozzle. It can be found from Fig. 5.4-(a) that the jet is penetrated more when it is introduced vertically than that in horizontal orientation. This may be due to the fact that, in the vertical orientation, the frontal area of the spray exposed to the cross-flow is less than that in the horizontal case, which causes a reduced interaction by solids convection. Another factor that may contribute to the orientation effect is from the thermal entrainment of the spray that dominates the spray evaporation and hence the penetration. The quick cooling by the evaporation in the side and wake regions of the spray tends to yield less entrained thermal energy in the vertical orientation than that in the horizontal case. Result shows that the effect of aspect ratio has a significant impact on the penetration length and trajectories of the spray jet under the

operating conditions. The increasing aspect ratio also causes the penetration length to increase. Penetration length agrees very well with each other and the deflection has differences at the end of penetration length but it the distance of the deviation is 87z/D so it is negligible.

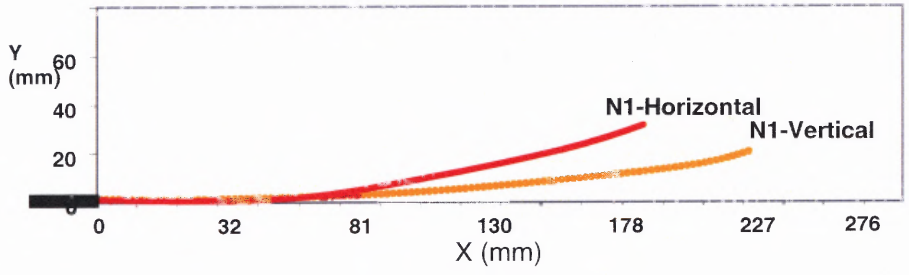

(a) Evaporation trajectory experimental results, nozzle: N-1 (aspect ratio 3)

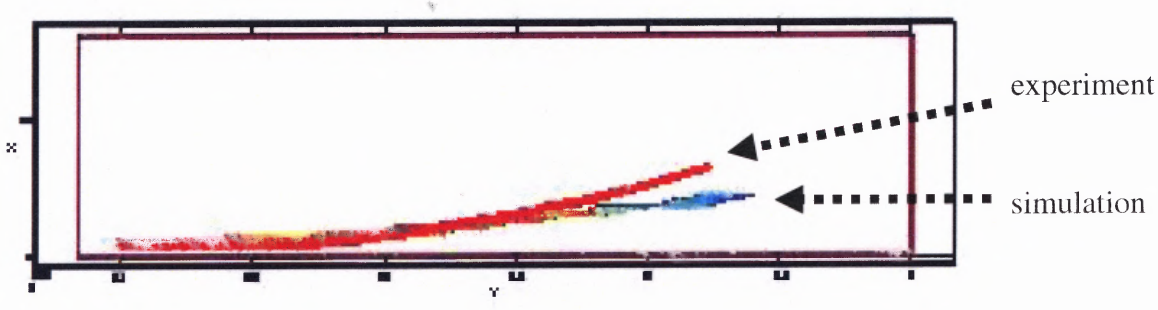

(b) Comparison of experimental and simulation results; horizontal nozzle case

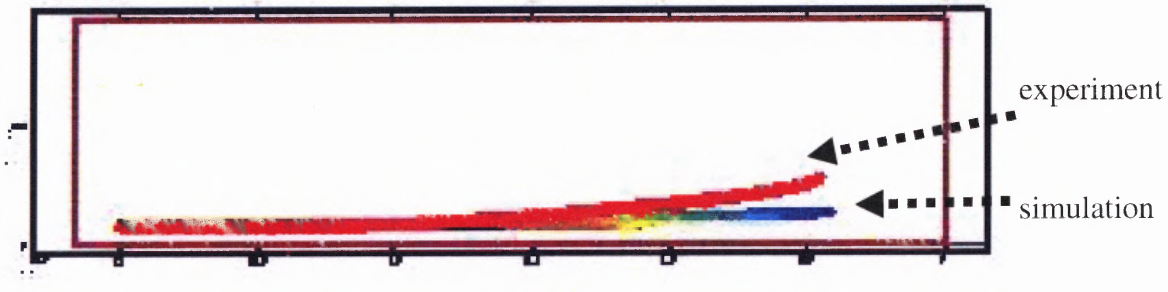

(c) Comparison of experimental and simulation results; vertical nozzle case

Figure 5.4 Verification of simulation with experimental results

5.3 Typical Phase Distributions

For this phase distribution, Case-1 in operations table has been used.

5.3.1 Evaporation Droplet Size Distribution

Following picture show droplet evaporation trajectory and droplet size with color.

Vertical plane was made on the center of the jet so the trajectory only shows the centerline trajectory of droplet trajectory.

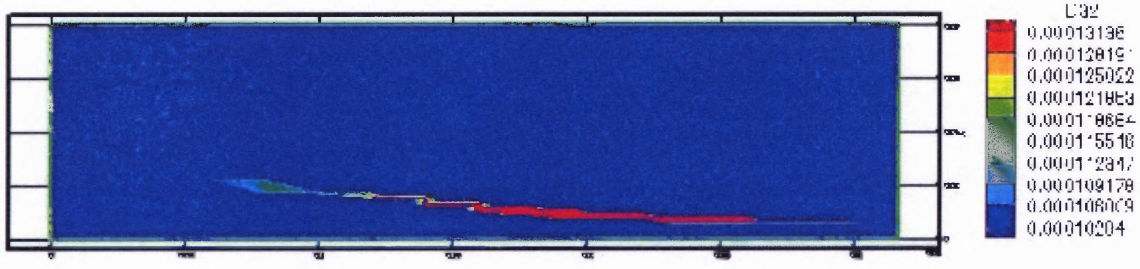

(a) Front view

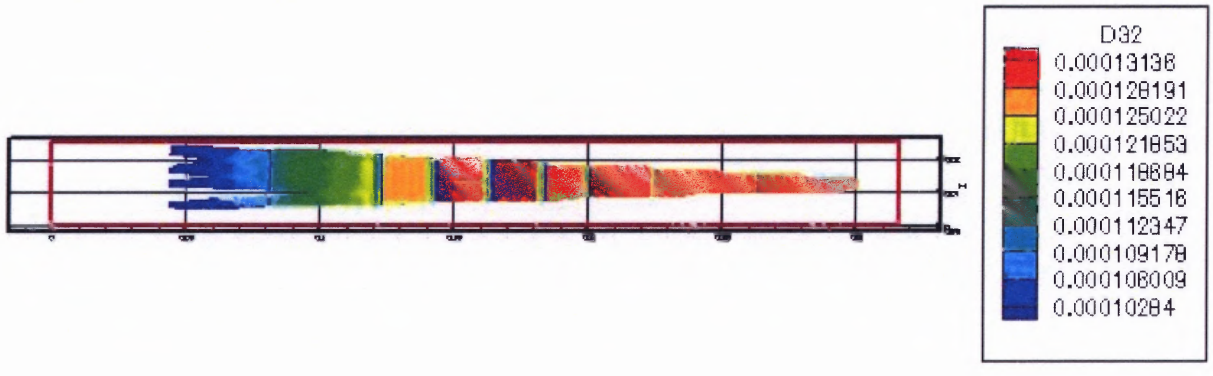

(b) Top view

Figure 5.5 Evaporation droplet size distributions with 1% solid.

5.3.2 Phase Velocities

The rapid evaporation of liquid spray in a gas-solid flow results in an excessive vapor production that is mixed into the surrounding gas stream, which not only changes the local velocities of gas and solids but also produces a dilution of solids concentration.

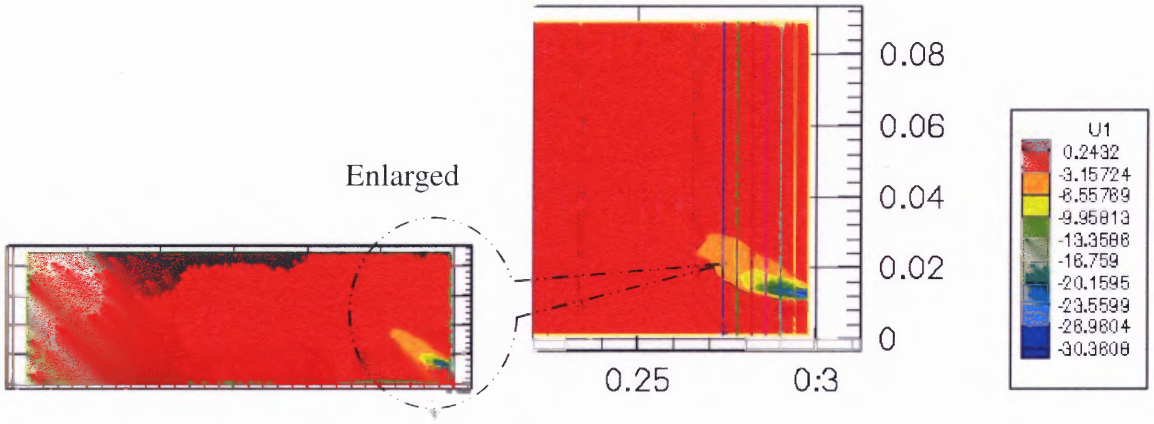

(a) Gas velocity contour overall front view

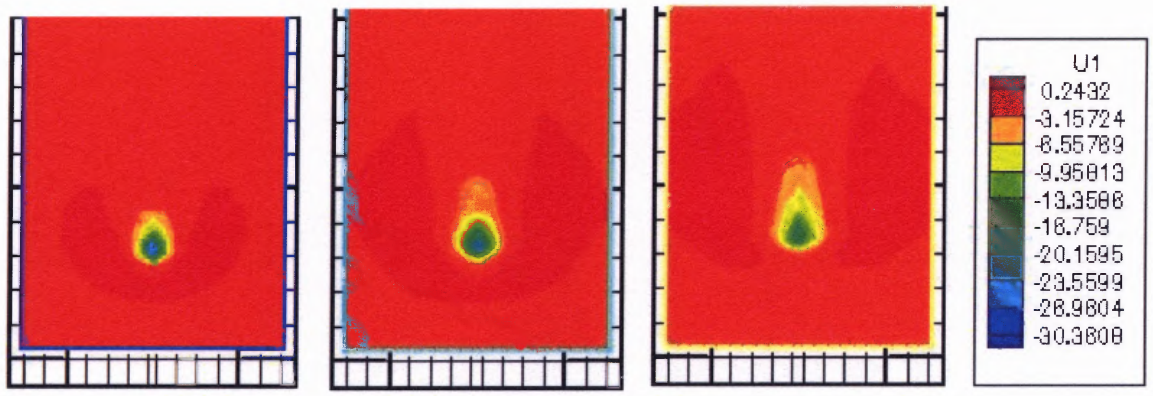

z/D = 2.4 z/D =4.8 z/D = 7.2

(b) Solid velocity contour changes along with distance from the nozzle

Figure 5.6 Phase velocity contours.

5.3.3 Gas/Solids Temperature Distributions

It is noted that lowest temperature distribution deviates the droplet trajectory while the droplet goes straight towards the other side wall. The trajectory of droplet is same with the temperature and phase velocity in the concurrent jet. Hence, a big temperature jump near the end of jet evaporation can define the evaporation length but for the cross-flow jet condition, we can not use the definitions any more. Detail things will be discussed in section 5.3.3.

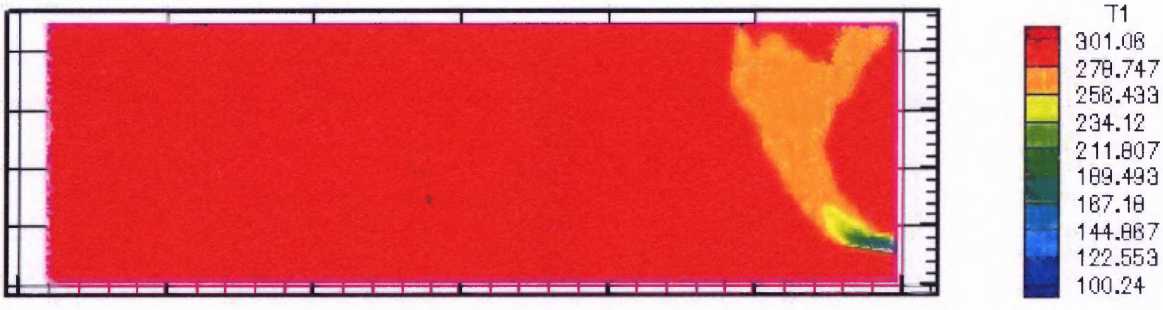

(a) Gas temperature contour (overall)

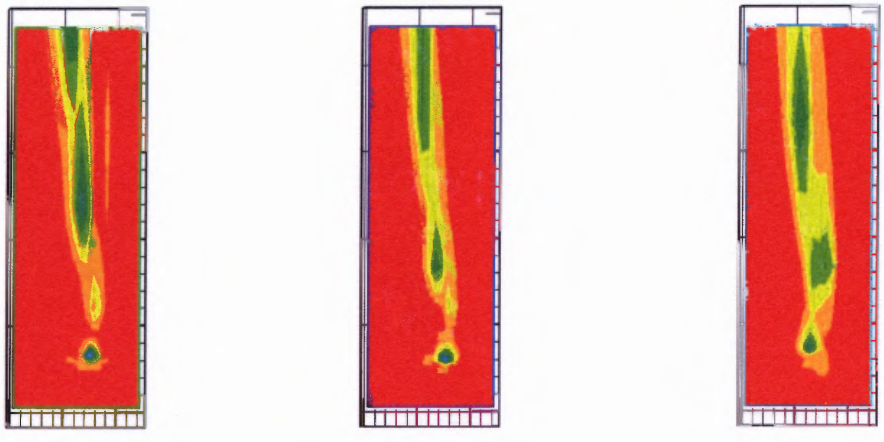

z/D=2.4 z/D= 4.8 z/D=7.2

(b) Gas temperature contour along with the distance from nozzle

Figure 5.7 Gas temperature distributions.

5.3.4 Particle Concentration

Figure 5.8 illustrates the dilution effect of solids in the evaporation region. There is a condense layer of solids (7-8%) surrounding the vapor region (which agrees with our experimental observation and measurements) whereas there is a diluted solids concentration (1-2%) within the vapor region. This is due to the vapor expansion by spray evaporation that pushes solids away from the spray region and, in the meantime, the solids are moved downstream by cross-flow convection. The vapor expansion also slightly increases the solids concentration in the confined chamber.

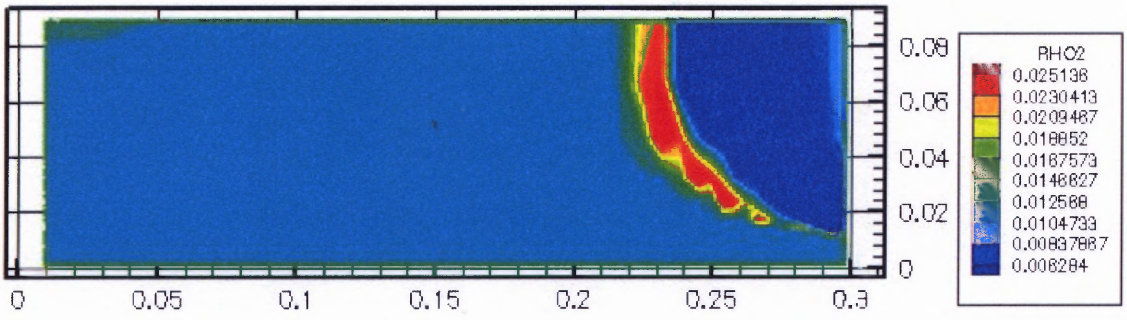

Figure 5.8 Particle concentration distribution.

5.4 Effect of Solid Concentration

5.4.1 Effect of Solid Concentration on Evaporation and Structure

Effect of solids loading on spray evaporation length is shown in Figure 5.9, which shows that the spray structure is significantly altered by the solids loading. The evaporation length with 5% volume fraction of solids is about 25% shorter than that without solids. Figure 5.11 gives the distribution of mass percentage of remaining droplet along the

spray trajectory. It is shown that, with solids, spray evaporates much faster, for example, about 60% of total evaporation occurs within one third of spray region for case of 5% solids while the same percentage evaporated over two third of spray region for case without solids.

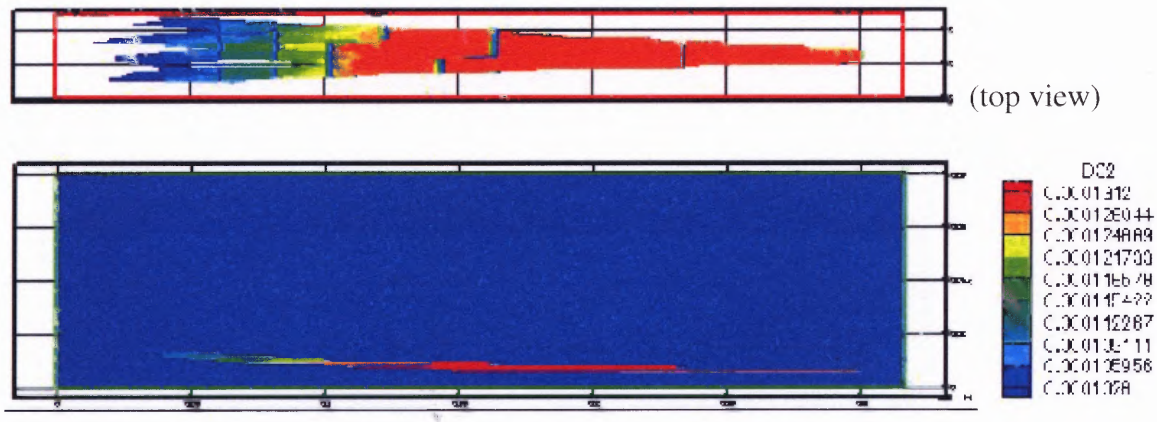

(a) Evaporation length without solid

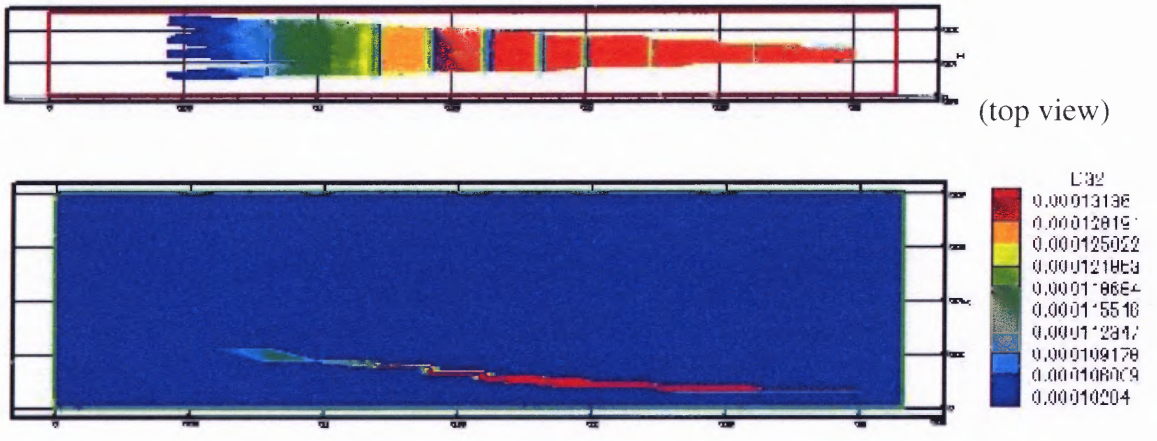

(b) Evaporation length with 1% solid loading

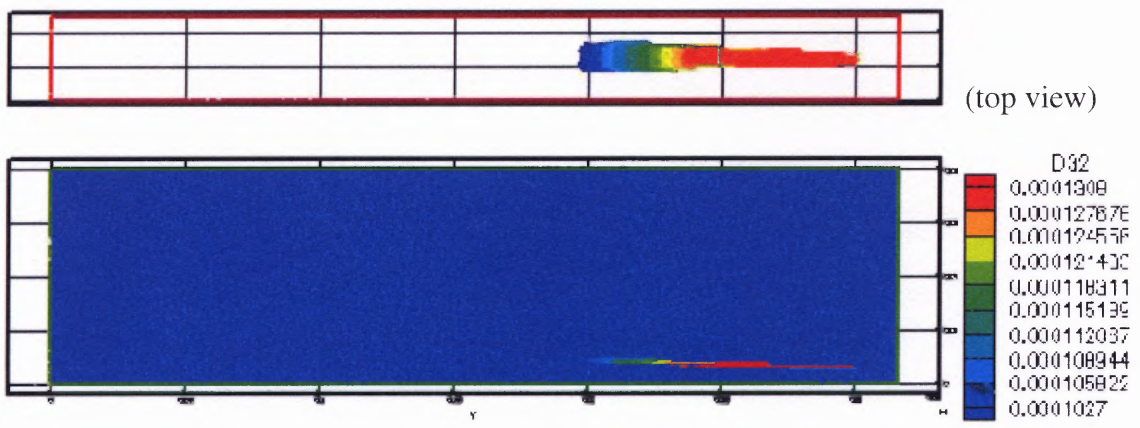

(c) Evaporation length with 15% solid

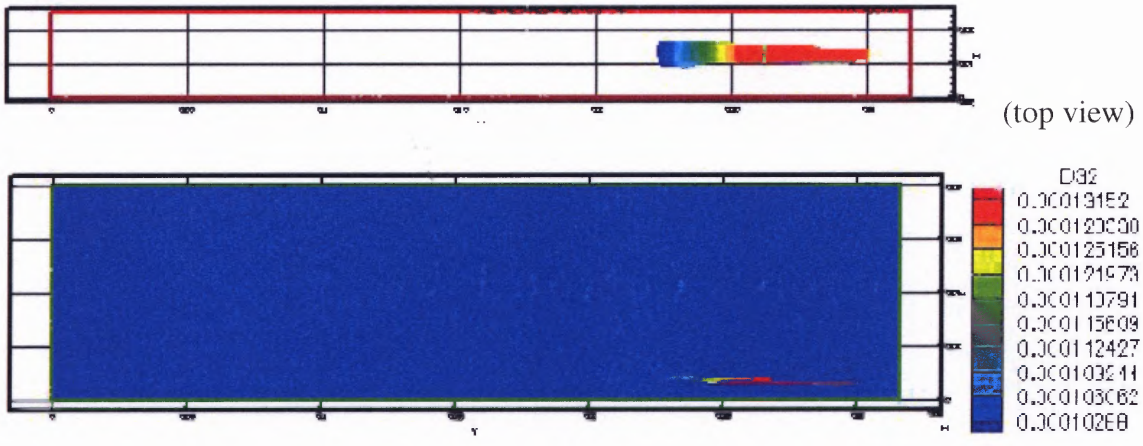

(d) Evaporation length with 25% solid

Figure 5.9 Effect of solid concentration on evaporation and structure.

Based on the information from above pictures, following graph was made. When there is no solid the evaporation rate is linear but even with 1% solid loading the rate eventually changed. It is noticed that there are not mush differences between 5% , 15% and 25%. Therefore the big change occurs in between with solid and without solid cases.

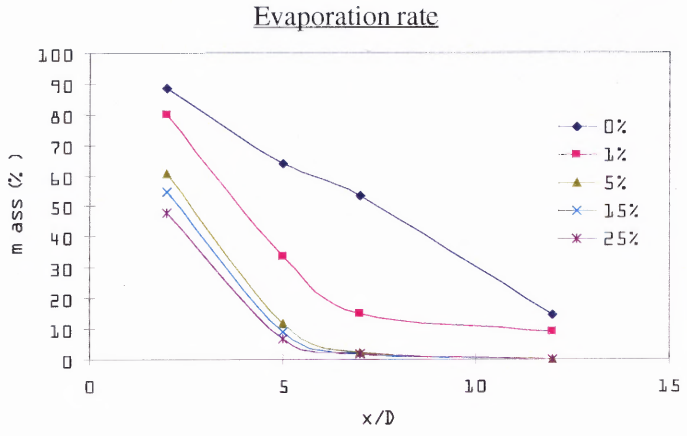

Figure 5.10 Evaporation rate with 0%, 1%, 5%, 15% and 25% solid.

5.4.2 Effect of Solid Concentration on Gas Velocity

Figure 5.12 shows the gas velocity distribution under the influence of droplet evaporation. It is shown that the gas velocity inside the vapor region has a sharp increase compared to the ambient velocity (2 m/s). The gas velocity pattern is similar to the temperature contour of gas. Compared with spray regions in Figure 5.10, it is once again noted that the vapor region is significantly deviated from the spray region by the strong cross-flow convection.

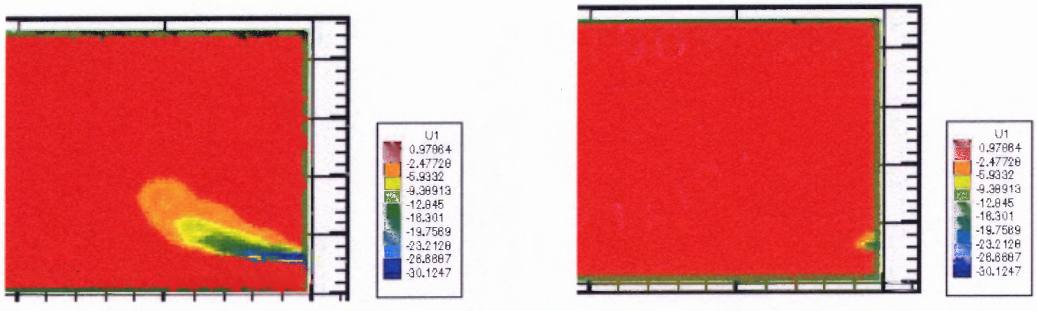

(a) Gas velocity without solid (b) Gas velocity with 15% solid

Figure 5.11 Effect of solid concentration on gas velocity.

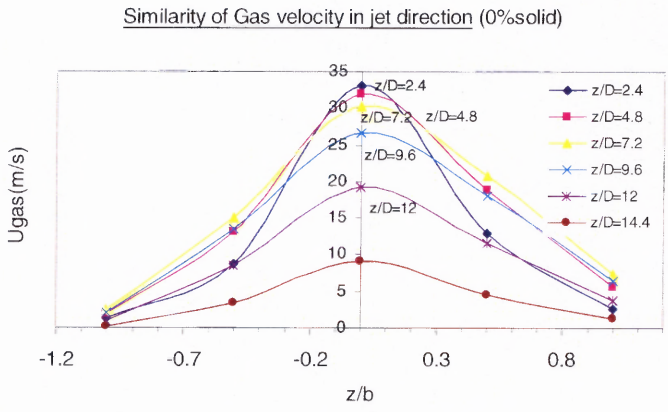

(a) Similarity of gas velocity at 0% solid loading

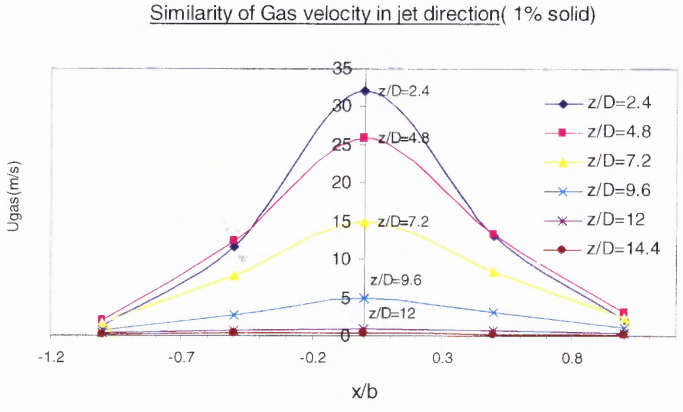

(b) Similarity of gas velocity at 1% solid loading

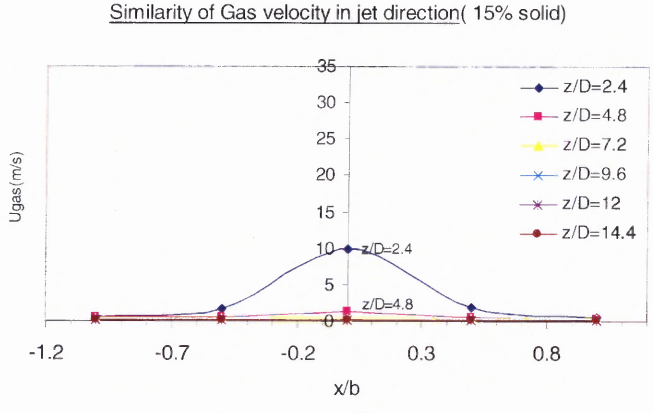

(c) Similarity of gas velocity at 15% solid loading

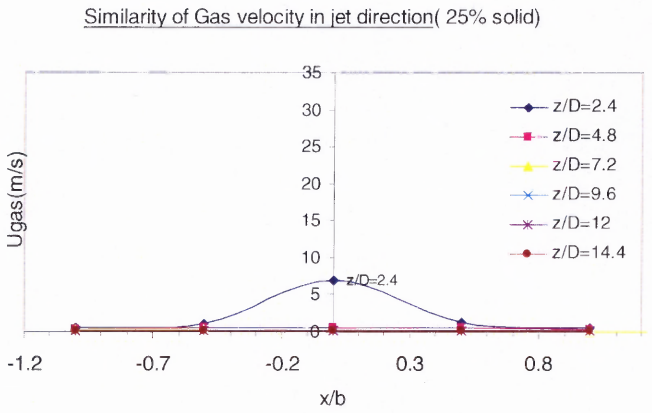

(d) Similarity of gas velocity at 25% solid loading

Figure 5.12 Similarity profiles on gas velocity at various solid loadings.

Maximum gas velocity in jet direction profile occurs above droplet trajectories. It's already deviates but the similarity of the gas velocity still holds. Only until in 7.2z/D distance, the maximum gas velocity location is in the droplet trajectory region. Again, the maximum gas velocity is not in the droplet trajectory region though, its profile in the droplet trajectory region has strong similarity.

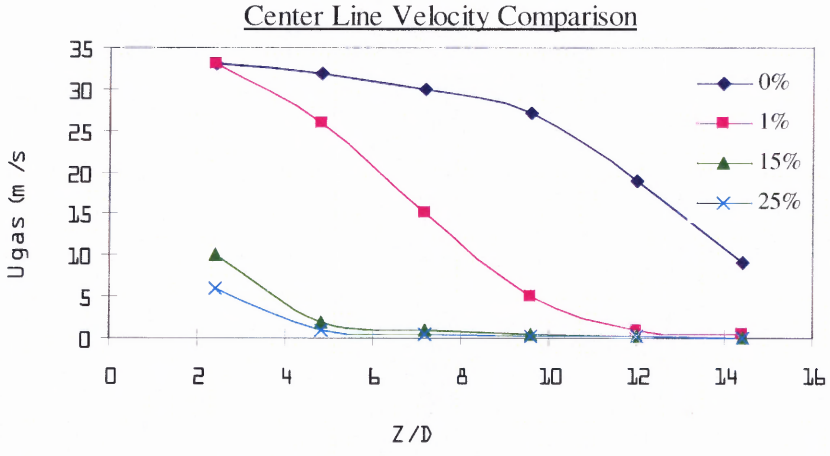

Figure 5.13 Gas velocity profiles at center position of droplet trajectory.

Gas velocity: strongly holds in 0%, 1% cases within 7.2 z/D distance and slightly holds till 14.4 z/D distance. For 15% cases, only within 2.4 z/D distance, there is a similarity but for other cases, there is no holds. For 25% cases, there is no holds at all. Figure 5.13 shows the velocities of droplet centerline of each case.

5.4.3 Effect of Solid Concentration on Gas Temperature

Droplet evaporation in a gas-solid flow also leads to a temperature reduction of the gas and solids due to the absorption of latent heat from the surrounding gas-solid media. The mixing effect of gas-solids at higher temperature and the evaporated nitrogen vapor at lower temperature also contributes to the temperature depletion.

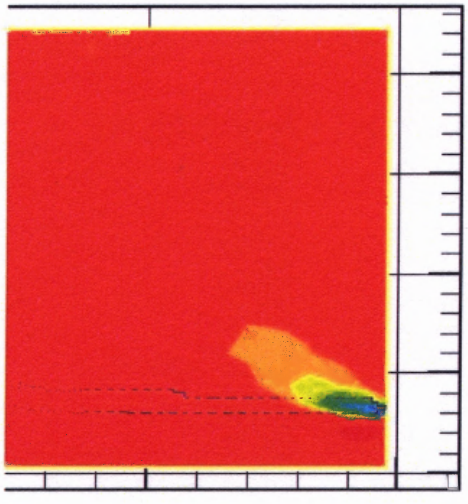

Figure 5.14 Deviation of temperature with droplet trajectory.

Figure 5.15 (a) and (b) illustrate the effect of solids loading on temperature distributions of gas and solids, respectively. It is noted that lowest temperature distribution deviates the droplet trajectory while the droplet goes straight towards the

other side wall. This result is different from our previous numerical results with co-current jet evaporation in which case the temperature contour of gas/solids represents that of spray evaporation region. The main reason for this deviation is the cross-flow convection. Due to their inertia, droplet keep going straight very much along the original injection direction but the evaporated vapor quickly engulfed into the wake region formed by gas-solids convection over the spray trajectory.

The lowest temperature distribution for case without solids appears at the half of the calculation domain whereas for the case of 5% (volume based) solids loading, the lowest temperature is shown above near the nozzle tip. This shows that more solid loading has the larger convection heat transfer to the cross direction. It is also interesting to note that, for case without solids, there exists a large low temperature region near the opposite side of the spray. This is due to the large recirculation of evaporated vapor in a confined chamber flow when the thermal convection of pipe flow is weak. The existence of this large low-temperature region is verified from our experimental measurements. Temperature depletion up to 50 K is obtained in solids phase. The profile of 25% is very small comparing with other cases and has similar patterns with 15% case so it is not listed here.

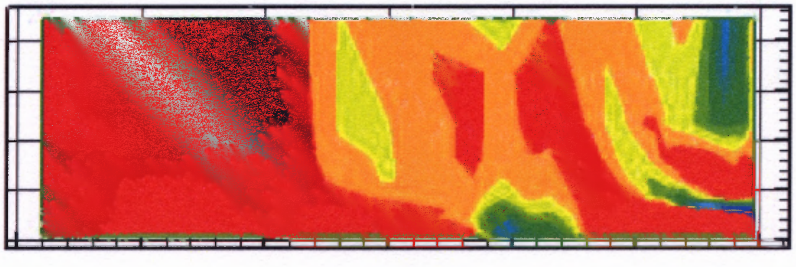

(a) Gas temperature without solid

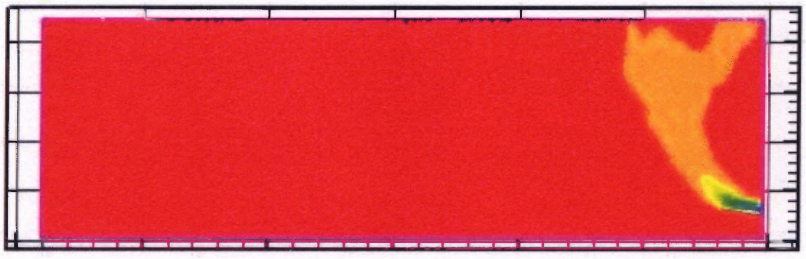

(b) Gas temperature with 1% solid

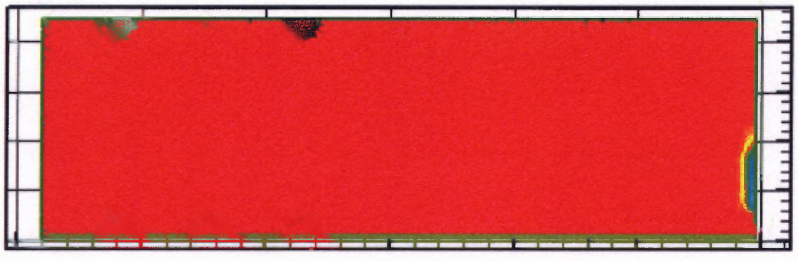

(c) Gas temperature with 15% solid

Figure 5.15 Effect of solid concentration on gas temperature.

The similar explanation is applied for the gas temperature similarity. Gas temperature strongly holds in 0%, 1% cases within 7.2 z/D distance and slightly holds till 14.4 z/D distance but in 15% and 25% cases similarity hold exists in very short distance.

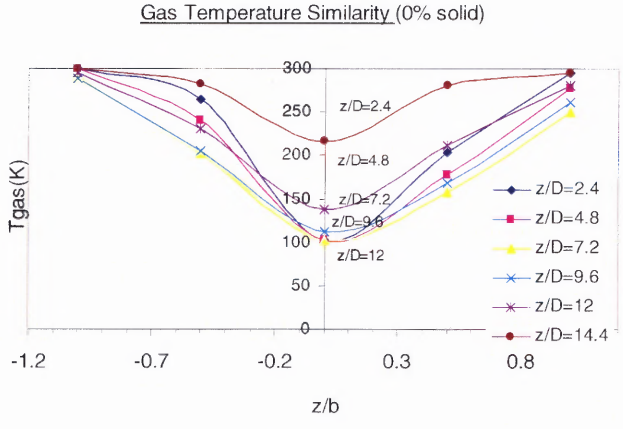

(a) Similarity of gas temperature at 0% solid loading

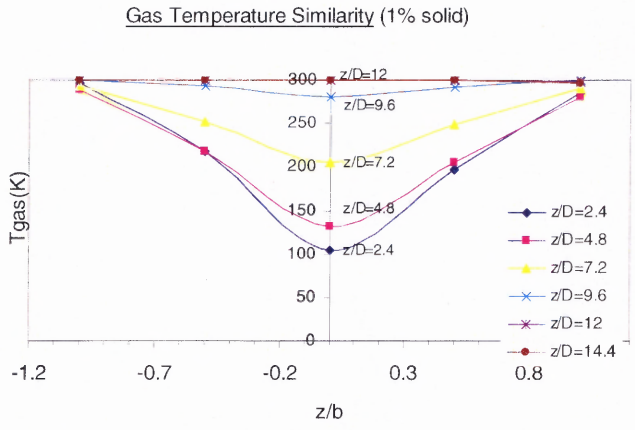

(b) Similarity of gas temperature at 1% solid loading

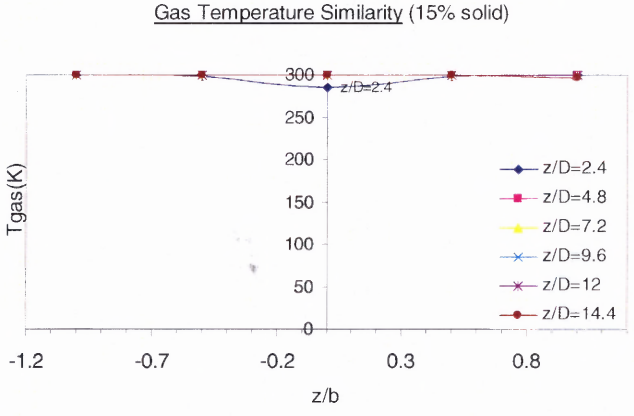

(c) Similarity of gas temperature at 15% solid loading

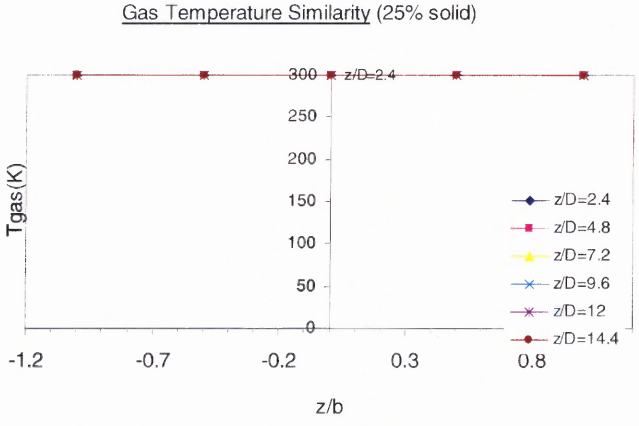

(d) Similarity of gas temperature at 25% solid loading

Figure 5.16 Similarity profiles on gas temperature at various solid loadings.

5.4.4 Effect of Solid Concentration on Particle Concentration

With spray evaporation, the solids concentration in the vapor region is diluted from 5% to 1.2%. There is a condense layer of solids (7-8%) surrounding the vapor region. For this case, different legends were used because its range is too different. Comparing to other case the 25% case is very small and has the similar pattern with 15% case so the contour picture is not listed here.

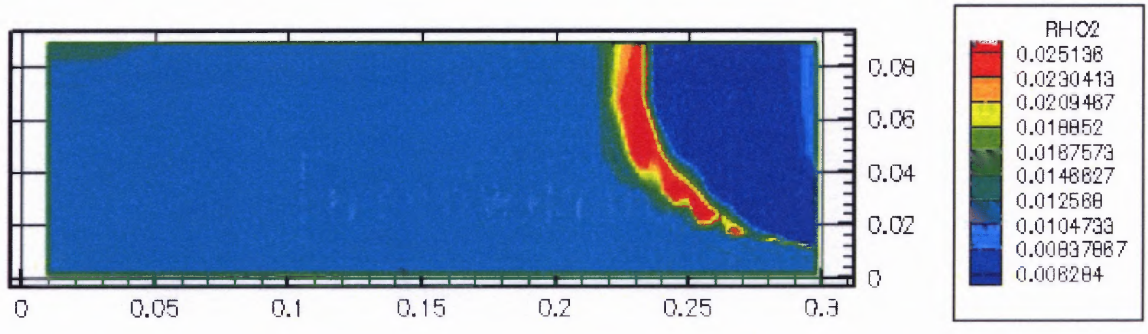

Figure 5.17 Solid volume fraction profile at 1% solid loading.

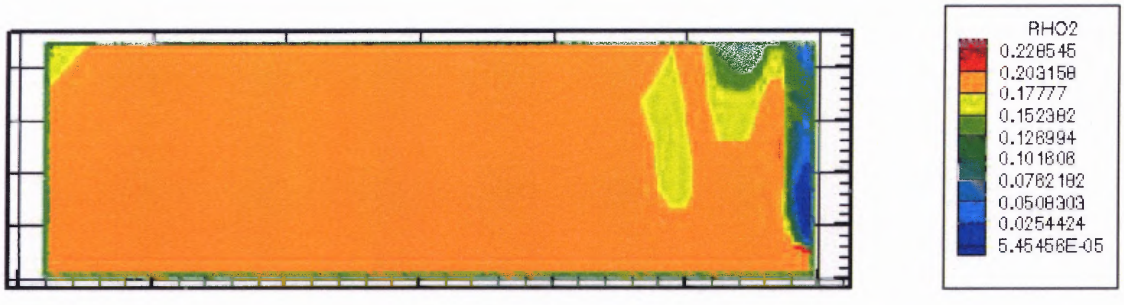

Figure 5.18 Solid volume fraction profile at 15% solid loading.

Solid concentration has different patterns depending on the distance from the nozzle and it shows the evaporation boundaries of each case very clearly.

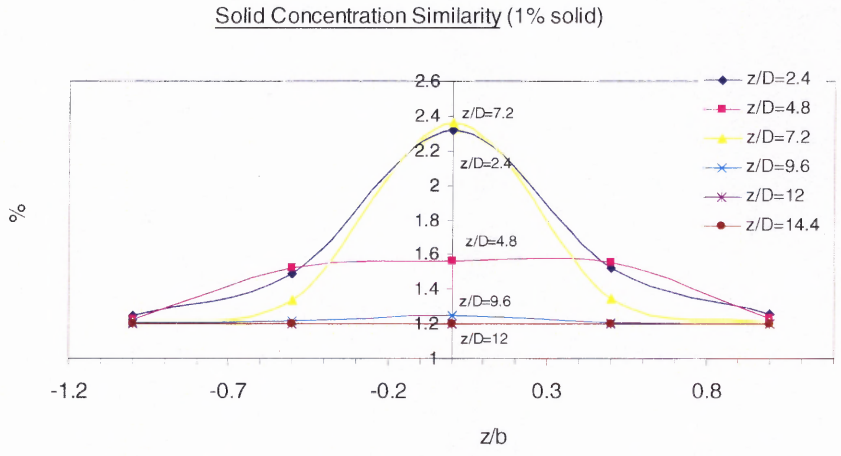

(a) Similarity of solid volume fraction at 1% solid loading

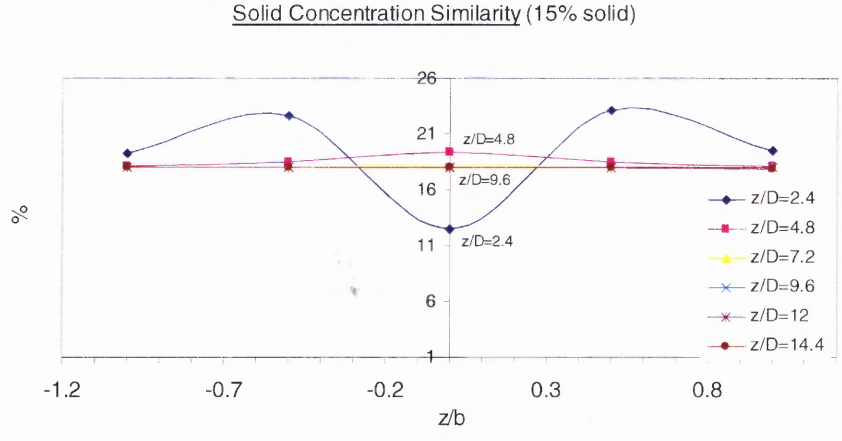

(b) Similarity of solid volume fraction at 15% solid loading

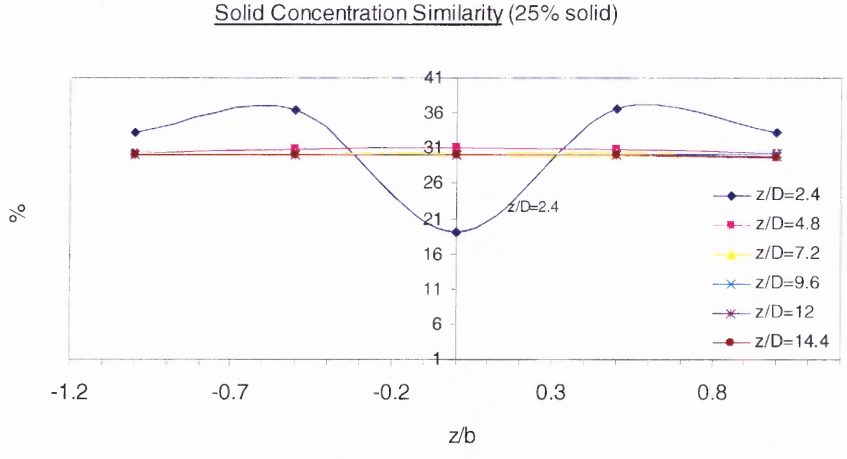

(c) Similarity of solid volume fraction at 25% solid loading

Figure 5.19 Similarity profiles on solid concentration at various solid loadings.

5.5 Jet Orientation Effect on Evaporation

5.5.1 Variations of Cross-Sectional Areas

For this study 10 cross- sections were selected along the droplet trajectory and the contour of each plane was investigated.

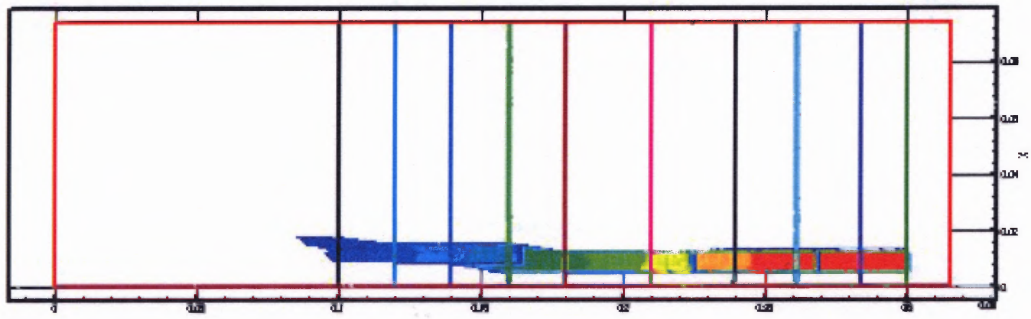

Figure5.20 Location of ten cross-section planes.

Table 5.4 Evaporation cross-section area at each plane.

	Droplet Evaporation cross-section at each plane		
Plane No.	Particle Concentration 0%	Particle Concentration 5%	Legend
1	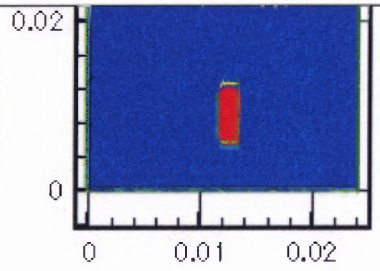	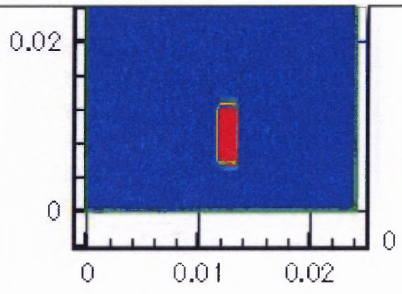	

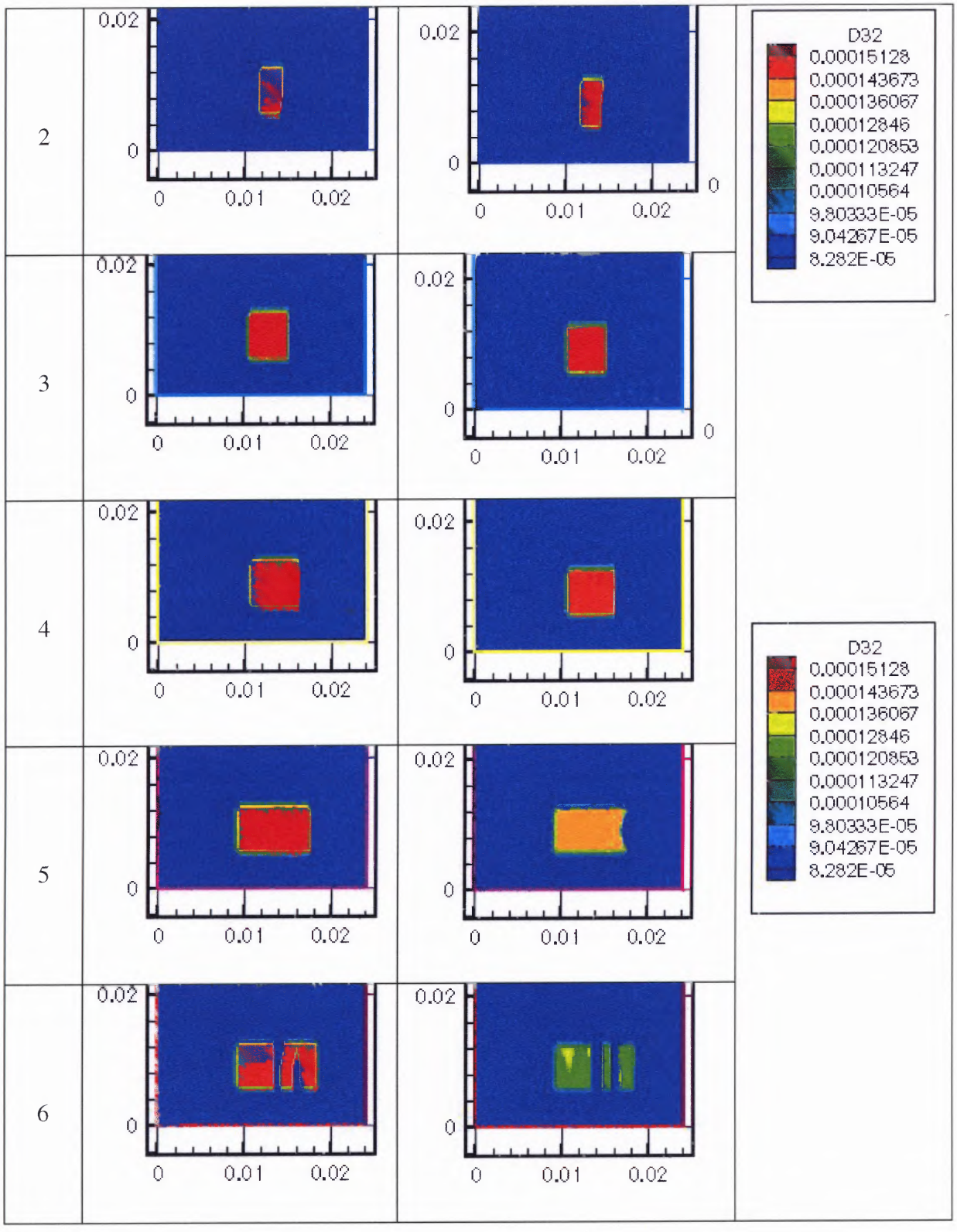
2
3
4
5
6
0.02
0
0
0.01
0.02
D32
0.00015128
0.000143673
0.000136067
0.00012846
0.000120853
0.000113247
0.00010564
9.80333E-05
9.04267E-05
8.282E-05

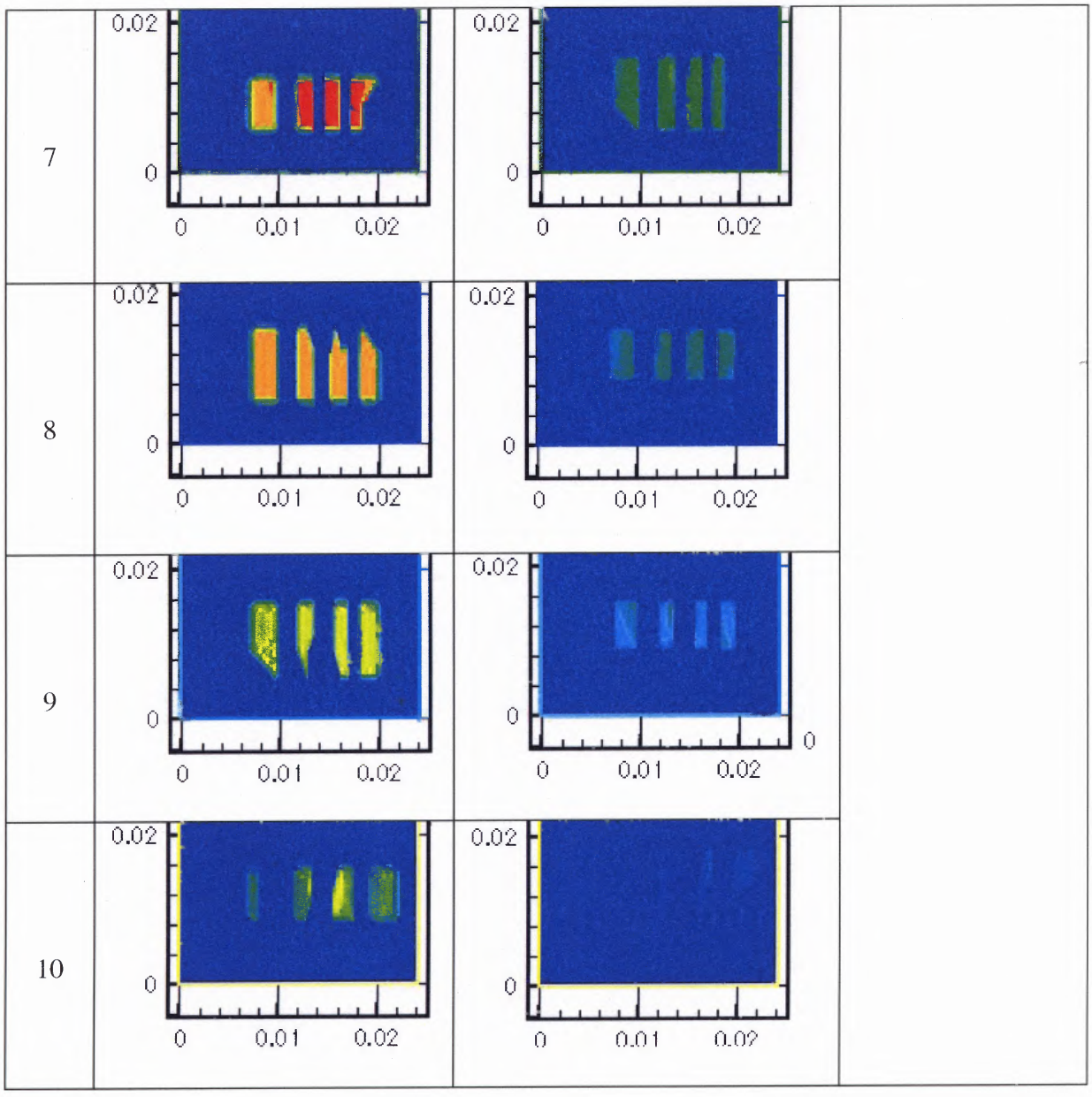

5.5.2 Aspect Ratio Analysis of Evaporation Expansion

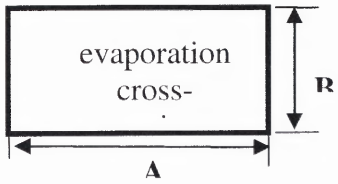

Figure 5.21 Definition of aspect ratio for a evaporation cross-section area.

Table 5.5 Aspect ratio for an evaporation cross-section area.

cross-section Number	0% solid			5% solid		
	A	B	A/B	A	B	A/B
1	2.0	9.0	0.2	2.0	9.0	0.2
2	3.0	8.5	0.4	2.5	9.0	0.3
3	4.5	8.3	0.5	5.0	8.5	0.6
4	6.0	8.2	0.7	6.0	8.2	0.7
5	9.0	8.0	1.1	8.4	8.0	1.1
6	10.1	8.0	1.3	10.0	7.8	1.3
7	14.0	8.0	1.8	11.5	10.0	1.2
8	14.0	9.2	1.5	12.5	7.5	1.7
9	13.8	9.2	1.5	12.7	7.0	1.8
10	15.5	7.8	2.0	16.0	8.0	2.0

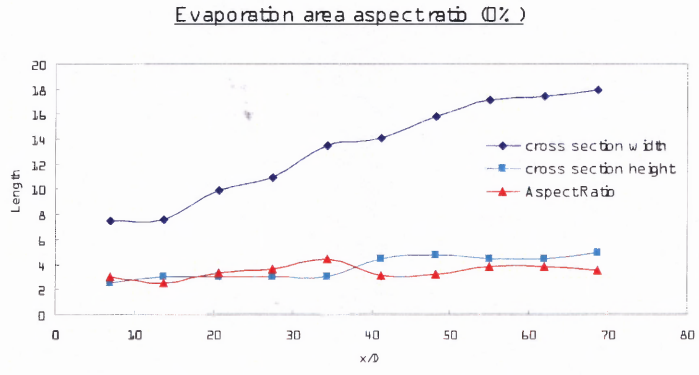

(a) Aspect ratio of evaporating area at solid loading 0%

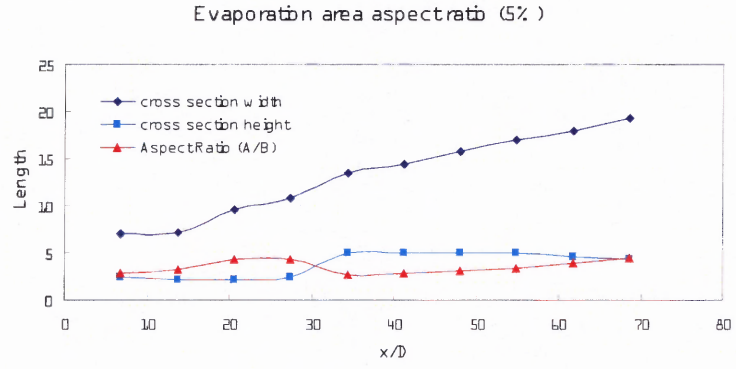

(b) Aspect ratio of evaporating area at solid loading 5%

Figure 5.22 Aspect ratio change for the evaporating area at solid loading 0% and 5%.

Table 5.5 Aspect ratio for an evaporation cross-section area.

cross-section Number	0% solid			5% solid		
	A	B	A/B	A	B	A/B
1	2.0	9.0	0.2	2.0	9.0	0.2
2	3.0	8.5	0.4	2.5	9.0	0.3
3	4.5	8.3	0.5	5.0	8.5	0.6
4	6.0	8.2	0.7	6.0	8.2	0.7
5	9.0	8.0	1.1	8.4	8.0	1.1
6	10.1	8.0	1.3	10.0	7.8	1.3
7	14.0	8.0	1.8	11.5	10.0	1.2
8	14.0	9.2	1.5	12.5	7.5	1.7
9	13.8	9.2	1.5	12.7	7.0	1.8
10	15.5	7.8	2.0	16.0	8.0	2.0

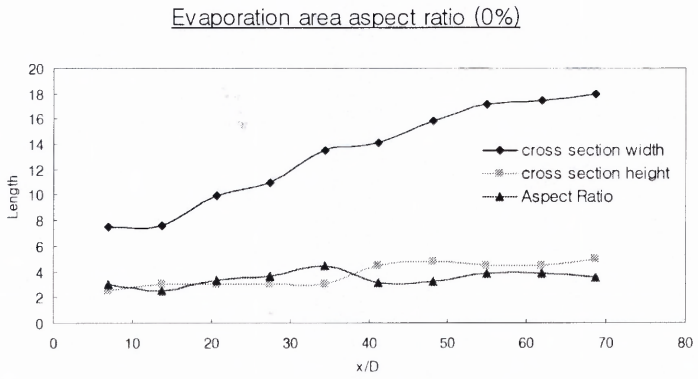

(a) Aspect ratio of evaporating area at solid loading 0%

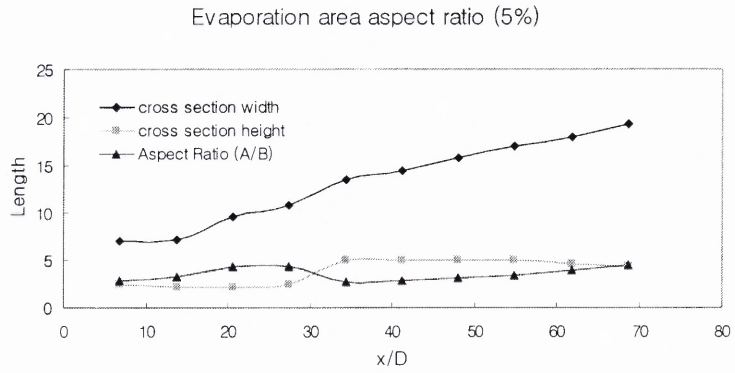

(b) Aspect ratio of evaporating area at solid loading 5%

Figure 5.22 Aspect ratio change for the evaporating area at solid loading 0% and 5%.

Based on information it is noticed that width of evaporation is increased linearly but the height remains almost same length with its original. More important thing is the aspect ratio. Its ratio also keeps the original values for this 5% case.

CHAPTER 6

SUMMARY AND CONCLUSIONS

Three dimensional full-field numerical simulations have been performed for the cross-flow liquid nitrogen sprays into a rectangular gas-solid fluidized bed. The effect of different solid volume fraction on the penetration length and jet deflection is investigated. The solids loading is shown to have a significant impact on both spray evaporation length and spray structure. The capacity of numerical calculation for three phase flow with three dimensions was verified by experimental results.

The results show that the spray penetrates basically along its injection fan angle but deflected by the gas-solid cross-flow convection. The penetration length is significantly reduced by the increase in solids loading. With an ambient solids loading of 5% (by volume), the evaporation length is about 25% shorter than without solids and 60% of evaporation already occurs within one thirds of total spray penetration length. Due to the strong cross-flow convection, most vaporized gas is significantly blown away from the spray region, as indicated by the downstream-directed deviation of the velocity and temperature contours of gas and solids.

The results also show that the spray evaporation leads to a very low solids concentration within the vapor region while there is a dense layer of solids surrounding the vapor region. With spray evaporation, the solids concentration in the vapor region is diluted from 5% to 1.2% while the temperature depletion up to 50 K is obtained in solids phase. There is also a condense layer of solids (7-8%) surrounding the vapor region, which agrees with our experimental observation and measurements.

Detailed droplet structure along the trajectory and field distributions of velocity, temperature and concentration of gas and solids were also obtained. With low solids concentrations, there exist flow similarities in velocity and temperature distributions in the spray region. Gas temperature strongly holds in 0%, 1% cases within 7.2 z/D distance, slightly holds till 14.4 z/D distances and in 15% and 25% cases similarity hold exists in very short distance. The flow structure is also strongly dependent on the nozzle orientation. The decreasing aspect ratios of the rectangular nozzles cause the penetration length to increase. The evaporating liquid spray jets, produced from the vertical configuration of rectangular nozzles, are penetrated longer for gas-solid cross-flows and are more deflected for the horizontal configuration of the nozzles. The simulation predictions agree reasonably well with the experimental measurements.

REFERENCES

1. Abramowitz, G.. M. , The Theory of Turbulent Jets. MIT Press.

2. Aggarwal, S. K., Tong, A. Y. and Sirignano, W. A., "A Comparison of Vaporization Models in Spray Calculations," *AIAA Journal*, 22, 1984, pp. 1448-1457.

3. Aluwalia, R., "Droplet Vaporization Model and FCC Riser Model", Argonne National Laboratory, March 1999.

4. Bazile R. and Stepowski, D. , "2D Laser Diagnostics of Liquid Methanol for Investigation of Atomization and Atomization and Vaporization Dynamics in a Burning Spray Jet", 25th Symposium (International) on Combustion Proceedings. July 1994, Irvine, CA, USA, p. 363.

5. Bojic, M. L. and Eskinazi, S. , "Two-dimensional model of a non buoyant jet in a cross flow", AIAA J. 17, 1979, pp. 1050-1054.

6. Buchanan, J. S. , " Analysis of Heating and Vaporization of Feed Droplet in Fluidized Catalytic Cracking Risers", *Ind. Eng. Chem. Res.* , vol. 33, 1994, pp. 3104-3111.

7. Chen, M. , Kontomaris, K. and McLaughlin, J. B "Direct Numerical Simulation of Droplet Collisions in a Turbulent Channel Flow. Part 1. Collision Algorithm", *International Journal of Multiphase Flow*, vol. 24, 1998, pp. 1079~1103.

8. Chang, S. L. , Lottes, S. A. , Zhou, C. Q. and Petrick, M. , "Evaluation of Multi-phase Heat Transfer and Droplet Evaporation in Petroleum Cracking Flows", HTD-vol. 335, Proceeding of ASME Heat Transfer Division 4, ASME 1996, pp. 17-27.

9. Coelho, S. L. V. and Hunt, J. C. R. "The dynamics of the near field of strong jets in cross flows", Journal of Fluid Mech. 200, 1989, pp. 95-120.

10. Cyrille Mirgain, Cedric Briens, Mariano Del Pozo, Roben Loutaty, Maurice Bergougnou, "Modeling of Feed Vaporization in Fluid Catalytic Cracking, Ind.Eng.Chem. Res.39, 2000, pp. 4392-4399.

11. Demuren, A. O. and Rodi, W. "Three-dimensional numerical calculations of flow and plume spreading past cooling towers", J. Heat Transfer 109, 1987, pp. 113-119.

12. Dubrovsky V. V. , Podvysotsky, A. M., A. A. Shraiber, " Particle Interaction in the Three-Phase Polydisperse Flows", *Int. J. Multiphase Flow*, vol. 68, 1992, pp. 337-352.

13. Elperin T., Krasovitov, B., " Radiation, Thermal Diffusion and Kinetic Effects in Evaporation and Combustion of Large and Moderate Size Fuel Droplet", *Int. J. Heat Mass Transfer*, vol. 38, 1995, pp. 409-418.

14. Fairweather, M., W. P. Jones and A. J. Marquis, "Predictions of the concentration field of a turbulent jet in a cross flow", Combust. Sci. Technol. 62, 1988, pp. 61-76.

15. Field, M. A., "Entrainment into an Air Jet Laden with Particles", *BCURA Inf.*, Circular No. 273, 1963.

16. Grandmaison, E. W. , Poollard, A. and Scalar, S. Ng, "Mixing in a free, turbulent rectangular jet", Int. J. Heat Mass Transfer 34, 1991, pp. 2653-2662.

17. Hinze, J. O., "Turbulent Fluid and Particle Interaction", *Prog. Heat Mass Transfer*, vol. 6, 1971, pp. 433~452.

18. Isaac, K. M. and Schetz, J. A., "Analysis of multiple jets in a cross flow", J. Fluids Engineering 104, 1982, pp. 489-492.

19. Jenkins, J. M. , Jones, R. L. , Jones, T. M. , Beret, S. , "Method for fluidized bed polymerization", *U.S. Patent* 4,588,790, 1986.

20. Jinsen Gao, Chunming Zu, Shizioug Lin, Guanghua Yang. "Simulations of Gas-Liquid–Solid 3-Phase Flow and Reaction in FCC Riser Reactors", AICHE Journal vol. 47, No. 3. Mar 2001.

21. Kouremenos, D., Pantzas, C., Panagalis, G., and Krikelis, R., Thermodynamics and the Design, Analysis, and Improvement of Energy Systems, 35, 1995, pp.261-273.

22. Krothapalli, A. , Lourenco, L. and Buchlin, J. M. , "Separated flow upstream of a jet in a cross flow", AIAA J. 28, 1990, pp. 414-420.

23. Makihata, T. and Miyai, Y. , Trajectories of Single and Double Jets Injected into a Cross flow of Arbitrary Velocity Distribution", J. Fluids Engng 101, 1979, pp. 217-223.

24. Pratte, D. and Baines, W.D., "Profiles of the round jet in a cross flow", J. Proc. Amer. Soc. Civil Engineering 93, HY-6, 1967, pp. 53-64.

25. Patrick, M.A., "Experimental investigation of the mixing and penetration of a round turbulent jet injected perpendicularly into a transverse stream, Trans". Inst. Chem. Engineers 45, T16 T31, 1967.

26. Rajaratnam, N., Turbulent Jets, Developments in Water Science(Chapter 9), Elsevier Science, 1976.

27. Sirignano, W. A., Fluid Dynamics and Transport of Droplet and Sprays. Cambridge University Press, 1999.

28. Skouby, D.C., "Hydrodynamic Studies in a 0.45-m Riser with Liquid Feed Injection". Proc. AICHE Annual Meeting, 1998, p. 238.

29. Sterland, P. R., and Hollingsworth, M. A., "Experimental study of multiple jets directed to a cross-flow", J. Mech. Engng Sci. 17, 1975, pp. 117-124.

30. Syamlal, M., Rogers, W. and O'Brien, T. J., "MFIX Documentation Theory Guide", Morgantown Energy Technology Center, *DE94000087*, Morgantown, WV, 1994.

31. Syamlal, M. , "MFIX Documentation User's Manual", Morgantown Energy Technology Center, *DE95000031*, Morgantown, WV, 1995.

32. Warsito, W. , and Fan, L.-S., Neural network based multi-criteria optimization image reconstruction technique for imaging two- and three-phase flow systems using electrical capacitance topography. Instrumentation Technique, 2001.

33. Weston, R. P. and Thames, F. C., "Properties of aspect ratio 4 rectangular jets in a subsonic cross flow", J. Aircraft 17, 1979, pp. 701-707.

34. Zhu, C. , Wang, X. and Fan, L.-S. , "Effect of Solid Concentration on Evaporative Liquid Jets in Gas-Solid Flows", Powder Technology, 111, 2000, pp. 79-82.

35. Zhu, C., Liu, G.. , Wang, X., and Fan, L.-S. , "A similarity model of evaporating liquid spray jets in concurrent gas-solid flows". Powder Technology, 119, 2001, pp. 292-297.

36. Zhu, C., Wang, X. , Liu, G.. , "Effect of Particle Loading on Liquid Nitrogen Jet Mixing in a FCC Riser". Circulating Fluidized Bed Technology VII. pp. 881-888.